Quarterly Reviews of Biophysics **35**, 4 (2002), pp. 327–367. © 2002 Cambridge University Press
DOI: 10.1017/S0033583502003840 Printed in the United Kingdom

Protein dynamics studied by neutron scattering

Frank Gabel[1], Dominique Bicout[2], Ursula Lehnert[1,2,3], Moeava Tehei[1], Martin Weik[1] and Giuseppe Zaccai[1,2,*]

[1] Institut de Biologie Structurale, 41 rue Jules Horowitz, 38027 Grenoble Cedex 1, France
[2] Institut Laue-Langevin, 6 rue Jules Horowitz, BP 156, 38042 Grenoble Cedex 9, France
[3] Max Planck Institut für Biochemie, D-82152 Martinsried, Germany

Abstract. This review of protein dynamics studied by neutron scattering focuses on data collected in the last 10 years. After an introduction to thermal neutron scattering and instrumental aspects, theoretical models that have been used to interpret the data are presented and discussed. Experiments are described according to sample type, protein powders, solutions and membranes. Neutron-scattering results are compared to those obtained from other techniques. The biological relevance of the experimental results is discussed. The major conclusion of the last decade concerns the strong dependence of internal dynamics on the macromolecular environment.

1. Introduction 328

2. Basic concepts of neutron scattering 329
2.1 Introduction 329
2.2 Neutron-scattering functions 331
2.3 Coherent and incoherent neutron scattering. The particular role of hydrogen in incoherent scattering 332
2.4 Total elastic scattering, EISF and mean square displacement (MSD) 333
2.5 Quasielastic scattering and relaxation function 334
2.6 Inelastic scattering and density of states 335

3. Experimental aspects and instruments 335
3.1 Energy and space resolution 335
3.2 General sample aspects 335
3.3 Potential effects of D_2O on dynamics 336
3.4 Experimental ^2H (deuterium) labelling 336

4. Physics of protein dynamics 336
4.1 Models 336
4.2 The dynamical transition 338
4.3 Effective force constants 339

5. Dynamics of hydrated protein powders 339
5.1 First experiments on myoglobin 340
5.2 Dynamical transitions in other proteins 340
5.3 The role of hydration water 341

* Address for correspondence: Giuseppe Zaccai, Institut de Biologie Structurale, 41 rue Jules Horowitz, 38027 Grenoble Cedex 1, France.
Tel.: +33 (0)4 38 78 95 73; Fax: +33 (0)4 38 78 54 94; E-mail: zaccai@ibs.fr

https://doi.org/10.1017/S0033583502003840 Published online by Cambridge University Press

5.4 Influence of the solvent 344
5.5 Diffusional motions within proteins by QENS 346
5.6 Inelastic neutron scattering and vibrational spectra 347
5.7 Conclusions 351

6. Membranes 352
6.1 Lipid bilayers 353
6.2 BR and the purple membrane (PM) 353
6.2.1 The dynamical transition in the PM 353
6.2.2 QENS from oriented PM 354
6.2.3 Hydration dependence of PM motions 355
6.2.4 Local dynamics in PM studied by isotope labelling 356
6.2.5 Dynamics of different BR conformations 357

7. Protein solutions 358
7.1 From powders to solutions 358
7.2 Water dynamics and solvent dependence of the dynamical transition in proteins 359

8. Comparing neutron scattering with other techniques 359

9. Biological relevance 360
9.1 Dynamics–activity relations 360
9.2 Dynamics–stability relations (adaptation to extreme environments) 360
9.3 Protein folding 361

10. Acknowledgements 364

11. References 364

1. Introduction

Thermal neutrons constitute a particularly useful radiation probe to study molecular dynamics (MD) in proteins, and its relation to biological function and activity. Thermal neutron wavelengths ($\sim$Å) and energies ($\sim$meV) correspond to inter-atomic distances and the energy of thermal excitations, respectively, so that neutrons are sensitive simultaneously to the amplitudes and frequencies of molecular motions. Furthermore, absorption is low for protein atoms (see Section 2.1) and they penetrate deeply into the sample, even for wavelengths $\sim$10 Å, which for X-rays, for example, are strongly absorbed. Neutron nuclear scattering cross sections are similar for most elements. Important isotope effects, in particular for H (hydrogen) and ^{2}H (deuterium or D), make them very powerful in the study of water and complex systems that can be selectively deuterium-labelled.

Neutron studies of protein dynamics were reviewed in this journal in 1991 by Smith, who discussed first experimental results in terms of the theoretical understanding of MD in proteins. Here, after sections on basic concepts of neutron scattering, experimental aspects and

Abbreviations: BLA, bovine α-lactalbumin; BR, bacteriorhodopsin; D, deuterium; DBLA, denatured bovine α-lactalbumin; DPPC, dipalmitoyl phosphatidylcholine; DTT, dithio-1,4-threitol; EISF, elastic incoherent structure factor; EL, elastic; GDH, glutamate dehydrogenase; H, hydrogen; *Hm*MalDH, *Haloarcula marismortui* malate dehydrogenase; HWHM, half-width at half-maximum; IE, inelastic; ILL, Institut Laue-Langevin; IQNS, incoherent quasielastic neutron scattering; KWW, Kohlrausch–William–Watts; MBLA, molten globule bovine α-lactalbumin; MD, molecular dynamics; MSD, mean square displacement; PM, purple membrane; QE, quasielastic; QENS, quasielastic neutron scattering; RH, relative humidity; SOD, superoxide dismutase.

https://doi.org/10.1017/S0033583502003840 Published online by Cambridge University Press

instruments, we review experiments on hydrated protein powders, membranes and protein solutions published up to early 2002, in Sections 5–9. We chose to discuss results in these terms because of the constraints imposed by sample requirements – typically $\sim$100 mg of material – and because the results of the last decade have established that protein dynamics is also dependent on the environment (hydration, solvent properties) and therefore on sample type. The energy resolution, Q-range and sample state are described in detail for each experiment reviewed. Progress in understanding the physics and biological significance of protein dynamics are addressed in Sections 4 and 9, respectively.

2. Basic concepts of neutron scattering

2.1 Introduction

Neutrons from a nuclear reactor or spallation source are moderated to be at thermal equilibrium close to room temperature with a typical energy of $\sim$25 meV; they are called thermal neutrons. 'Cold' neutrons, which are obtained by equilibration at very low temperatures ($\sim$20 K) in a 'cold source' allow shifting of the peak flux to higher wavelengths and have typical energies of $\sim$2·5 meV. Due to their dispersion relation,

$$E = \frac{\hbar^2}{2m}\frac{1}{\lambda^2}, \tag{1}$$

and their mass

$$m = 1{\cdot}67 \times 10^{-27}\ \text{kg}, \tag{2}$$

the corresponding wavelength λ, is close to 1 Å (10^{-10} m).

Neutrons are characterized by their energy

$$E = \hbar\omega \tag{3}$$

and their momentum

$$\mathbf{p} = m\mathbf{v} = \hbar\mathbf{k} \tag{4}$$

(where $\mathbf{k}$ is the wave vector, $k = 2\pi/\lambda$).

Neglecting electromagnetic interactions (cf. Sears, 1986), an incident neutron will undergo one of three processes when it encounters a sample. (1) The neutron passes through the sample without changing its physical characteristics (which is in general the case for most of the neutrons in a scattering experiment due to their relatively low interaction probability with matter). (2) It is absorbed in a nuclear process and its energy is dissipated. For usual nuclei in proteins, the main reactions are $^{1}\text{H(n,}\gamma)^{2}\text{H}$, $^{14}\text{N(n,p)}^{14}\text{C}$. They are considered negligible in neutron-scattering experiments because of their very low probability for the wavelength range 1–10 Å, even though each reaction deposits a substantial amount of energy. (3) The neutron is scattered by a nucleus, exchanging momentum and energy (inelastic scattering, $\Delta E \neq 0$) or just momentum and conserving energy (elastic scattering, $\Delta E = 0$) with the sample:

$$\Delta E = \hbar(\omega' - \omega), \tag{5}$$

$$\Delta\mathbf{p} = \hbar(\mathbf{k}' - \mathbf{k}) = \hbar\mathbf{Q}, \tag{6}$$

where primed and unprimed quantities are after and before the scattering event, respectively, and $\mathbf{Q}$ is the momentum transfer (in units of $\hbar$).

https://doi.org/10.1017/S0033583502003840 Published online by Cambridge University Press

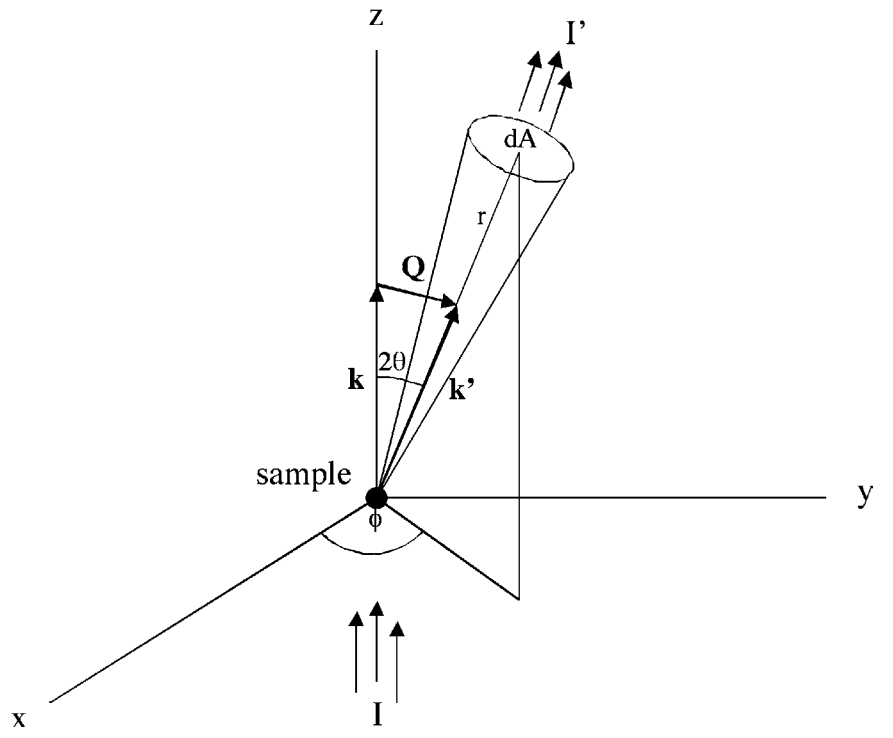


Fig. 1. Geometry for scattering by a single nucleus in three dimensions. The neutrons are scattered in the solid angle $d\Omega = dA/r$ under the scattering angle 2θ and the azimuthal angle ϕ.

Information on sample structure and dynamics is obtained by analysing the scattered beam as a function of momentum and energy transfer. Scattered neutrons are recorded by a detector as a function of the scattering angle. As neutron detectors are based on nuclear reactions between neutrons and detector nuclei (e.g. ^{3}He(n,p)^{3}H) they are not capable of resolving the neutron energy but only detect neutrons in a 'yes or no' event. In an experiment requiring energy resolution, the energy of the scattered beam has to be analysed (either by determining the wavelength by Bragg reflection from a crystal or by determining its velocity in a time-of-flight experiment) before it is counted in the detector.

The interaction between the neutrons and the sample takes place via the nuclei. It is due mainly to a short-range nuclear force and can be considered as a sudden collision between a neutron and a nucleus. The probability of a neutron being scattered in a unit solid angle (Fig. 1) is expressed in terms of the differential scattering cross section

$$\frac{d\sigma}{d\Omega} = \frac{I'}{I} = b^2. \tag{7}$$

It represents the average number of neutrons I', per unit time, that are scattered in the solid angle $d\Omega$ and per unit incident flux I (neutrons per area per time unit). b is the scattering length, representing an effective linear dimension of the scatterer. Units of b are in 10^{-15} m, much smaller than the neutron wavelength, so that the nucleus can be considered as a point and the scattering is isotropic. The total scattering cross section (usually given in units of barns, where 1 barn is 10^{-24} cm^2) is the integral of the differential scattering cross section in all directions (solid angle 4π):

https://doi.org/10.1017/S0033583502003840 Published online by Cambridge University Press

$$\sigma_t = \int_{4\pi} \frac{\mathrm{d}\sigma}{\mathrm{d}\Omega}\,\mathrm{d}\Omega = 4\pi b^2. \tag{8}$$

The scattering of a neutron being, in general, dependent on the energy exchange occurring during the impact, the concept of the differential scattering cross section can be extended to the double-differential cross section $\partial^2\sigma/\partial\Omega\,\partial\omega$ where

$$\int \frac{\partial^2\sigma}{\partial\Omega\,\partial\omega}\,\mathrm{d}\omega = \frac{\mathrm{d}\sigma}{\mathrm{d}\Omega}. \tag{9}$$

Information on sample dynamics is contained in the scattering function $S(\mathbf{Q},\omega)$ which is related via a spatio-temporal Fourier transform to the positions of the sample scattering nuclei as a function of time.

For a system of N identical atoms, this function is related to the double-differential cross section:

$$\frac{\partial^2\sigma}{\partial\Omega\,\partial\omega} = N\frac{k'}{k}b^2 S(\mathbf{Q},\omega). \tag{10}$$

The factor k'/k assures the conservation of the flux of neutrons before and after the sample (k, k' being proportional to incident and scattered neutron velocities, respectively).

2.2 Neutron-scattering functions

A neutron will exchange momentum and energy with appropriate states in the sample. Measurement of $S(\mathbf{Q},\omega)$ provides access to sample states as a function of energy and momentum. The probability of measuring scattered neutrons is dependent upon constructive interference of scattered waves from nuclei located at certain positions in space and time. The correlation function $g(\mathbf{r},t)$ describes the mutual positions of nuclei in the sample as a function of time. $g(\mathbf{r},t)$ is the Fourier transform in space and time of $S(\mathbf{Q},\omega)$ and can be split into two parts: (1) An autocorrelation function describing the trajectory of single nuclei and giving rise to incoherent scattering. (2) A correlation function describing different nuclei and giving rise to coherent scattering.

The scattering function (or dynamic structure factor) $S(\mathbf{Q},\omega)$ can be written as:

$$S(\mathbf{Q},\omega) = \frac{1}{2\pi}\int_{-\infty}^{+\infty} I(\mathbf{Q},t)\exp\{-i\omega t\}\,\mathrm{d}t \tag{11}$$

with the intermediate scattering function

$$I(\mathbf{Q},t) = \int_{-\infty}^{+\infty} g(\mathbf{r},t)\exp\{+i\mathbf{Q}\cdot\mathbf{r}\}\,\mathrm{d}\mathbf{r} = \frac{1}{N}\sum_{k,j}\langle \mathrm{e}^{i\mathbf{Q}\cdot\mathbf{r}_k(t)}\mathrm{e}^{-i\mathbf{Q}\cdot\mathbf{r}_j(0)}\rangle, \tag{12}$$

which is the space Fourier transform of the atomic correlation function (where the $\langle\ \rangle$ stand for ensemble averaging), N being the number of scatterers in the sample. The pair correlation function $g(\mathbf{r},t)$ is given by:

$$g(\mathbf{r},t) = \frac{1}{N}\sum_{k,j}^{N}\langle\delta\{\mathbf{r}+\mathbf{r}_k(0)-\mathbf{r}_j(t)\}\rangle. \tag{13}$$

https://doi.org/10.1017/S0033583502003840 Published online by Cambridge University Press

When evaluating the expression for the double-differential scattering cross section, it must be considered that the scattering lengths of the nuclei are associated with their positions. The expression $b^2S(\mathbf{Q},\omega)$ can be split into two terms after summation and thermal averaging over all atoms and spin states; one part being the sum of terms from individual nuclei, the other one containing only mixed terms:

$$\frac{d^2\sigma}{\mathrm{d}\Omega\,\mathrm{d}\omega} = \frac{1}{2\pi N}\frac{k'}{k}\int_{-\infty}^{+\infty} \times \left\{ \sum_k b_{\mathrm{inc},k}^2 \langle \mathrm{e}^{i\mathbf{Q}\cdot\mathbf{r}_k(t)}\mathrm{e}^{-i\mathbf{Q}\cdot\mathbf{r}_k(0)}\rangle + \sum_{k,j} b_{\mathrm{coh},k} b_{\mathrm{coh},j} \langle \mathrm{e}^{i\mathbf{Q}\cdot\mathbf{r}_k(t)}\mathrm{e}^{-i\mathbf{Q}\cdot\mathbf{r}_j(0)}\rangle \right\} \exp(-i\omega t)\,\mathrm{d}t. \quad (14)$$

The measured intensity therefore consists of the so-called *incoherent* part and the *coherent* part:

$$\frac{d^2\sigma}{\mathrm{d}\Omega\,\mathrm{d}\omega} = \frac{d^2\sigma_{\mathrm{inc}}}{\mathrm{d}\Omega\,\mathrm{d}\omega} + \frac{d^2\sigma_{\mathrm{coh}}}{\mathrm{d}\Omega\,\mathrm{d}\omega}, \quad (15)$$

$$\sigma_{\mathrm{tot}} S(\mathbf{Q},\omega) = \sigma_{\mathrm{inc}} S_{\mathrm{inc}}(\mathbf{Q},\omega) + \sigma_{\mathrm{coh}} S_{\mathrm{coh}}(\mathbf{Q},\omega). \quad (16)$$

2.3 Coherent and incoherent neutron scattering. The particular role of hydrogen in incoherent scattering

Scattering by a sample depends on the positions and dynamics of the many different nuclei as well as on the spin-dependence of the neutron–nucleus interaction. The scattered intensity is divided into two parts. A *coherent* part, which results from the interference of waves scattered by different nuclei, and an *incoherent* part, which is the difference between the total scattering and the coherent part. Incoherent scattering can be understood as waves scattered independently by individual atoms and interfering with themselves during a time-course which is defined in practice by the instrumental resolution. H has one of the largest incoherent cross sections of all nuclei.

At the origin of the incoherent scattering is the spin-dependence of the neutron–nucleus interaction. The neutron as well as the nucleus with which it interacts have intrinsic spins, **s** and **L**, with eigenvalues s ($=\frac{1}{2}$), and L, respectively. During the scattering act, the compound neutron–nucleus system can be described by the composite spin quantum number $J = L + s$. The scattering length depends on whether $J = L + \frac{1}{2}$ (associated with b^+) or $J = L - \frac{1}{2}$ (associated with b^-). The multiplicity of each state is given by $2J+1$. The mean value of the scattering length of a nucleus [corresponding to b_{coh} in Eq. (14)] is then given by

$$b_{\mathrm{coh}} := \langle b\rangle = \frac{L+1}{2L+1} b^+ + \frac{L}{2L+1} b^-, \quad (17)$$

whereas the incoherent scattering length of a nucleus results as the deviation from this mean value:

$$b_{\mathrm{inc}} := \sqrt{\langle b^2\rangle - \langle b\rangle^2}, \qquad \langle b^2\rangle = \frac{L+1}{2L+1}(b^+)^2 + \frac{L}{2L+1}(b^-)^2. \quad (18)$$

Neutron scattering from a non-crystalline biological sample is dominated by the incoherent scattering of the hydrogen nucleus (Bée, 1988). As pointed out by Smith (1991), in the time and space window of neutron-scattering experiments, the incoherent scattering by H atoms reflect

https://doi.org/10.1017/S0033583502003840 Published online by Cambridge University Press

the motions of the larger groups to which they are bound (e.g. methyl groups or amino-acid side-chains).

Two remarks concerning the incoherent cross section of hydrogen:

(1) At the origin of the unusually large incoherent scattering cross section of hydrogen are the values of the scattering lengths of the singlet (b^-) and triplet (b^+) intermediate neutron–proton state. The singlet neutron–proton state is energetically near a bound state (quasi-bound) and therefore possesses a very large negative-scattering length b^-, and a rather small positive-scattering length b^+ (Blatt & Weisskopf, 1952). This combination of scattering lengths contributes, via Eq. (18), to the exceptionally large incoherent scattering cross section of the hydrogen (^{1}H) nucleus.

(2) The incoherent hydrogen cross section varies for neutron energy ranging from 100 meV (wavelength $\sim$1 Å) to 1 meV ($\sim$10 Å). This is due to the effect of chemical binding and can be shown by a transformation between the laboratory and centre-of-mass system (Fermi, 1936) between bound and free-scattering cross section

$$\sigma_{\text{bound}} = \sigma_{\text{free}} \cdot \left(\frac{A+1}{A}\right)^2, \tag{19}$$

where A is the atomic mass number. Whereas for heavier nuclei this effect is present but weak, it is particularly strong for the hydrogen nucleus because its mass is almost equal to that of the neutron. As the transition between free and bound cross sections takes place in the energy range of thermal neutrons (10–30 meV) it has to be taken into account when calculating the contributions of different nuclei to the scattering intensity of a sample.

2.4 Total elastic scattering, EISF and mean square displacement (MSD)

The total elastic intensity (within instrumental resolution) as a function of the scattering vector contains information on the geometry of motions integrated over the time corresponding to the instrumental resolution. For example, if H-atom motions describe an ellipse in 100 ps, it will correspond to the scattering of an ellipse provided the instrumental resolution corresponds to a time of 100 ps or longer (energy resolution of about 10 μeV or better). The elastic incoherent structure factor (EISF) is defined as the fraction of the elastically scattered intensity with respect to the total intensity.

As the positions of the nuclei after a long time $\mathbf{r}_k(\infty)$, are uncorrelated to the initial positions $\mathbf{r}_k(0)$, for infinitely good energy resolution ($\Delta E = 0$), the total elastic intensity is described by the time-independent part of the intermediate scattering function:

$$I_{\text{inc}}(\mathbf{Q}, \infty) = \frac{1}{N} \sum_k |\langle e^{i\mathbf{Q}\cdot\mathbf{r}_k} \rangle|^2. \tag{20}$$

In the Gaussian approximation, the Fourier transform of Eq. (20) is

$$S_{\text{inc}}(Q, \omega = 0) = \exp\left[-\tfrac{1}{6}\langle u^2 \rangle Q^2\right]. \tag{21}$$

It is valid for the product $\langle u^2 \rangle Q^2$ smaller than $\sim$2, where $\langle u^2 \rangle$ is the atomic MSD. In this case, the obtained MSDs are independent of the model used to describe the potential governing the dynamics of the individual atoms.

https://doi.org/10.1017/S0033583502003840 Published online by Cambridge University Press

From Eq. (21), one obtains for the MSD:

$$\langle u^2 \rangle = -6 \frac{d \ln [S(\mathbf{Q}, \omega = 0)]}{d(Q^2)} \bigg|_{Q=0}. \tag{22}$$

Note the similarity of this formulation to the Guinier approximation in small-angle scattering (Guinier & Fournet, 1955), with $\langle u^2 \rangle/2$ being equivalent to the squared radius of gyration.

In practice, ω is not 0 because of finite instrumental energy resolution so that the MSDs calculated by using Eq. (22) are time-dependent. It is best experimentally to use an instrument with an appropriate energy resolution and Q-range so that the geometry of 'localized' diffusive motions (e.g. the motion of an H atom anchored to a protein via an amino-acid side-chain) is found well within the space–time window defined by the experiment.

The MSDs are only time-independent, as given by Eq. (22), for an instrument with infinitely good energy resolution. In the case of finite resolution, they can be described by the combination of time-independent parts $\langle u_\alpha^2 \rangle$ and a correlation function $C_\alpha(t)$ (Bicout & Zaccai, 2001), where the sum goes over all atoms.

$$\langle u^2(t) \rangle = -6 \frac{d \ln [I(\mathbf{Q}, t)]}{d(Q^2)} \bigg|_{Q=0} = \frac{1}{N} \sum_{\alpha=1}^{N} \langle u_\alpha^2 \rangle [1 - C_\alpha(t)]. \tag{23}$$

The time-dependence of the atomic movements is contained in the correlation function.

In contrast to the total elastic intensity, the EISF is experimentally accessible as the ratio of the elastically scattered intensity to the sum of elastically and quasielastically scattered intensity. This definition (e.g. Bée, 1988) of the EISF neglects inelastic scattering:

$$A_0(\mathbf{Q}) := \frac{S_{\text{inc}}^{\text{EL}}(\mathbf{Q})}{S_{\text{inc}}^{\text{EL}}(\mathbf{Q}) + S_{\text{inc}}^{\text{QE}}(\mathbf{Q})}. \tag{24}$$

The EISF is different from the total elastic intensity, which includes elastic and quasielastic scattering within the instrumental resolution at $\omega = 0$. The EISF is mainly used in quasielastic neutron-scattering (QENS) experiments to define the geometry of motions.

2.5 Quasielastic scattering and relaxation function

In quasielastic experiments, the scattered intensity is interpreted in the form of a Debye–Waller factor, the EISF, and the close-to-zero energy-transfer scattering from which information on the time-course of different motions can be obtained.

From the intermediate scattering function, split up in the EISF A_0 and a time-dependent part,

$$I(\mathbf{Q}, t) = A_0(\mathbf{Q}) + [1 - A_0(\mathbf{Q})] \Phi(\mathbf{Q}, t), \tag{25}$$

one obtains the expression for $S(\mathbf{Q}, \omega)$

$$S(\mathbf{Q}, \omega) = \exp\lfloor -\langle x^2 \rangle Q^2 \rfloor \cdot \{A_0(\mathbf{Q}) \delta(\omega) + [1 - A_0(\mathbf{Q})] S_{\text{QE}}(\mathbf{Q}, \omega)\}, \tag{26}$$

where the Debye–Waller factor, $\exp(-\langle x^2 \rangle Q^2)$, accounts for vibrational modes and S_{QE} is the quasielastic scattering centred on $\omega = 0$.

https://doi.org/10.1017/S0033583502003840 Published online by Cambridge University Press

2.6 Inelastic scattering and density of states

Inelastic scattering experiments to study vibrational spectra and the density of states have been discussed in detail by Smith (1991).

The density of states (in the limit $Q \to 0$), weighted by the atomic cross sections (b_l^2), masses (m_l) and squared displacement vectors (C_l^λ) is given by:

$$G(\omega) = \lim (Q \to 0) \frac{6\omega}{\hbar Q^2} \left(\exp\left\{ \frac{\hbar\omega}{k_B T} \right\} - 1 \right) S(\mathbf{Q}, \omega) = \sum_{\lambda, l} \frac{b_l^2 |C_l^\lambda|^2}{m_l} \delta(\omega - \omega_\lambda). \quad (27)$$

Because it is relevant to the data discussed below, we recall that in the case of a harmonic, infinite three-dimensional (3D) solid, at small scattering vectors describing wavelengths that are long with respect to inter-atomic distances (the continuum approximation), the density-of-states function is proportional to ω^2; this is the Debye law.

Taking into account elastic, quasielastic and inelastic scattering, the scattering function can be written as:

$$S(\mathbf{Q}, \omega) = \exp\lfloor -\langle x^2 \rangle Q^2 \rfloor \cdot \{\mathrm{EISF}(\mathbf{Q})\delta(\omega) + [1 - \mathrm{EISF}(\mathbf{Q})] S_{\mathrm{QE}}(\mathbf{Q}, \omega)\} + S_{\mathrm{IE}}(\mathbf{Q}, \omega). \quad (28)$$

3. Experimental aspects and instruments

3.1 Energy and space resolution

Neutron-scattering instruments are characterized by their energy resolution and available Q-range. The energy resolution, i.e. the instrumental energy width of the elastic peak, defines the 'time window' $\sim 1/\Delta E$ (when energy is expressed in frequency units) of the experiment, whereas the Q-range defines the 'space window' $\sim 1/Q$.

Depending on incident wavelength, backscattering instruments cover Q-values from lower than 0·1 to several $\mathrm{Å}^{-1}$ with an energy resolution from 1 to 10 μeV. Time-of-flight instruments present Q-ranges and energy resolution values that are also highly dependent on incident wavelength; with Q-values from the order of 0·001 $\mathrm{Å}^{-1}$ to almost 10 $\mathrm{Å}^{-1}$ and energy resolution from 1 μeV to 5 meV (Frick & Farago, 2002).

Because incident neutron beams are imperfectly monochromatic due to instrument characteristics, scattered intensity has to be corrected by deconvolution for the finite Gaussian-, Lorentzian- or triangle-like energy resolution (depending on the instrument type) before comparing the scattered intensity to the theoretical $S(\mathbf{Q}, \omega)$ scattering function.

3.2 General sample aspects

Biological samples used in energy-resolved neutron-scattering experiments have some particular features compared to samples used with other techniques. Required sample mass is rather large, ~ 100 mg. For incoherent scattering to be dominant, the samples should not include crystalline structures of any kind (salts, ice crystals, etc.), which would give large coherent peaks in the total scattering. Sample measuring times are typically of the order of approximate hours with the currently available fluxes at neutron sources. The temperature range chosen for elastic scans usually covers from ~ 10 to ~ 300 K for powder samples, and from above 273 K (0 °C) for solutions (to avoid freezing of the aqueous environment or crystallization of salt solutions).

In order to calculate a correct $S(\mathbf{Q}, \omega)$ from the experimental data, multiple scattering must

https://doi.org/10.1017/S0033583502003840 Published online by Cambridge University Press

be avoided or corrected for. This can be checked by a simple calculation. The mean free path l, of a neutron between two interactions is given by $l = 1/\sigma \cdot \rho$ where ρ is the density per unit volume and σ the average cross section of scattering units. To minimize the probability of multiple scattering the sample size L, has to be smaller than the mean free path ($L \ll 1$). As an extreme example, pure water (H_2O) with a scattering cross section of about $\sigma = 170 \times 10^{-24}$ cm^2 per water molecule for thermal neutrons (Bée, 1988) and a density of $3{\cdot}35 \times 10^{22}$ water molecules per cm^3 has a neutron mean free path $\sim 1{\cdot}8$ mm.

3.3 Potential effects of D_2O on dynamics

Solvent interactions provide a complex contribution to protein structure stabilization through hydration, van der Waals interactions, hydrogen bonds, ion binding, and the hydrophobic effect. Heavy water (D_2O) is often used as a solvent for proteins in neutron-scattering, NMR, and spectroscopic studies. H_2O and D_2O are molecules of almost identical dipole moment, shape, size, and bond lengths. However, the different masses, reduced masses, and moments of inertia make their vibrational and librational frequencies substantially different (Nemethy & Scheraga, 1964; Conway, 1981). D_2O displays a higher temperature of maximum density than H_2O, greater viscosity, and larger heat of vaporization and sublimation. For proteins, D_2O leads to stronger hydrogen-bond interactions as well as to lower solubility of apolar groups, which favours the hydrophobic interaction (Nemethy & Scheraga, 1964). In practice, D_2O stabilizes protein structures (Bonneté *et al.* 1994) and it has been shown to modify dynamics (Tehei *et al.* 2001). Extreme caution must therefore be exercised when D_2O is used as a contrast medium, for example, to reduce the scattering of water in order to study the motions of protein non-exchangeable hydrogens, because the protein motions themselves are likely to be affected.

3.4 Experimental ^{2}H (deuterium) labelling

Deuterium labelling of non-labile H atoms in biological systems has been used very successfully in neutron diffraction and small-angle scattering to study complex structures (Scherbakova *et al.* 1997; Weik *et al.* 1998). There are few examples of neutron dynamics studies on deuterium-labelled samples. Deuterated phycocyanin dynamics was studied by neutron scattering mainly to focus on the hydration water (Bellissent-Funel *et al.* 1996). In a dynamics study of labelled purple membranes (PMs) (see Section 6.2.4) by neutron scattering with energy resolution in the μeV range, the MSDs of the fully deuterated membrane were found to be similar to those of the natural abundance sample (Réat *et al.* 1998). In the space–time window of the experiment the scattering was sensitive to side-chain motions and not to the motions of individual H atoms with respect to the atoms to which they were bonded. And deuterating a CH_2, for example, changes its mass by less than 15%. There are not sufficient data, however, to conclude that deuterium labelling does not affect dynamics and careful control experiments should be performed in each case.

4. Physics of protein dynamics

4.1 Models

Several models describing atomic motions within proteins have been proposed to interpret neutron experimental data. They consist of potentials governing the movements of protein

https://doi.org/10.1017/S0033583502003840 Published online by Cambridge University Press

atoms and/or solvent/hydration atoms. Physical quantities such as the EISF and MSDs are predicted mathematically by models for comparison with the experiment. In a complementary approach, normal mode analysis has been used to describe atomic vibrations, from which $S(\mathbf{Q}, \omega)$ can be calculated (Smith, 1991, and references therein).

Two models that have been used preferentially to describe experimental data by neutron scattering, are presented below.

A two-state model was developed from Mössbauer spectroscopy (Mayo *et al.* 1981). The *double-well potential* model was introduced by Doster *et al.* (1989) (cf. Section 5.1) to interpret neutron-scattering data from a hydrated myoglobin powder. It describes the hydrogen motions up to a dynamical transition at about 200 K (see Section 4.2) by a vibrational (Debye–Waller) factor and at higher temperature by jumps between two sites separated spatially by a distance d, and energetically by a free energy ΔG. The resulting scattering function is

$$S(Q,0) = \mathrm{e}^{-Q^2\langle \Delta x^2\rangle_G}\left\{1 - 2p_1p_2\left(1 - \frac{\sin(Qd)}{Qd}\right)\right\}, \tag{29}$$

where

$$\langle \Delta x^2\rangle_G = \langle \Delta x^2\rangle - \tfrac{1}{3}p_1p_2d^2, \tag{30}$$

where $p_2/p_1 \sim \exp(-\Delta G/RT)$ is the population distribution ratio between wells. The model accounts quite well for elastic scattering curves, with μeV energy resolution, in a relatively wide range of Q (up to 4 or 5 Å^{-1}), as are available on IN13 at the Institut Laue-Langevin (Yellow Book, ILL), and for the behaviour observed for the MSDs as a function of temperature.

A *diffusion inside a sphere* model was introduced by Volino & Dianoux (1980). Each atom is assumed to diffuse freely inside a hard-walled (impermeable) sphere of radius a. The scattering law corresponding to this model is the sum of an elastic term (EISF) and a set of Lorentzians

$$S(Q,\omega) = \left[A_0(Q)\cdot\delta(\omega) + \frac{1}{\pi}\sum_{i=1}^{N}A_i(Q)\cdot\frac{\Gamma_i}{\Gamma_i^2+\omega^2}\right], \tag{31}$$

where Γ_i are the half-widths at half-maximum (HWHM) of the quasielastic components, with associated correlation times $\tau_i = \Gamma_i^{-1}$. Equation (31) is a model interpretation of Eq. (26), neglecting the Debye–Waller factor.

The EISF is given by

$$A_0(Q) = \left[\frac{3j_1(Qa)}{Qa}\right]^2 \tag{32}$$

which is the Q-dependence expected for the scattering from a solid sphere of radius a. $j_1(Qa)$ is the spherical Bessel function of the first order.

For Qa going to infinity (i.e. focusing on the geometry of the motions well inside the sphere, with very large values of Q or a), the scattering law represents diffusion according to Fick's law

$$S(Q,\omega) = \frac{1}{\pi}\frac{DQ^2}{[DQ^2]^2+\omega^2} \tag{33}$$

with an intermediate scattering function

$$I(\mathbf{Q},t) = \exp(-t/\tau), \tag{34}$$

https://doi.org/10.1017/S0033583502003840 Published online by Cambridge University Press

$$\frac{1}{\tau} = DQ^2, \tag{35}$$

where τ is the relaxation time. A modified version of this law is the KWW function

$$I(\mathbf{Q}, t) = \sum_{i=1}^{N} \exp(-t/\tau_i) \approx \exp(-t/\tau)^{\beta}. \tag{36}$$

with the stretching exponent β (Angell, 1995), which takes into account deviations from Fick's diffusion law. It has been used by various authors to describe diffusional atomic behaviour in proteins (cf. Section 5).

Various versions of the hard-sphere model have been used to describe the quasielastically scattered intensity and to deduce diffusion coefficients as well as relaxation times (Bellissent-Funnel *et al.* 1996, and references therein). Dellerue *et al.* (2001) applied a hard-sphere model in terms of a set of spheres of different radii.

Bicout & Zaccai (2001) proposed a model based on the theoretical work by Volino & Dianoux (1980) and mode-coupling theory (Götze & Sjögren, 1992), which describes the atomic potential as two concentric wells of different depths and a hard outer sphere of radii a and R, with $R > a$. Atomic motions are divided into two different populations, a fraction ϕ within the innermost sphere and $1-\phi$ within the outermost sphere. The EISF is given by

$$A(Q) = \left| \phi \left[\frac{3j_1(Qa)}{Qa} \right] + (1-\phi) \left[\frac{3j_1(QR)}{QR} \right] \right|^2 \tag{37}$$

and the MSD by

$$\langle u^2(T) \rangle = [1-\phi(T)] \frac{k_B T}{k_1} + \phi(T) \frac{k_B T}{k_2}. \tag{38}$$

where k_1 and k_2 are effective force constants (Section 4.3).

The above-mentioned models have been useful as a guide to experiments because they fit the data extremely well, but clearly they are 'wrong' as far as protein dynamics is concerned. MD simulations have clearly established, for example, that bound protein hydrogen atoms do not form a homogeneous population.

4.2 The dynamical transition

Upon cooling glass-forming liquids, several physical parameters undergo large changes at a temperature called the 'glass transition' temperature, T_g (Angell, 1995). The heat capacity C_p exhibits a steep decrease and the viscosity η, increases dramatically. This phenomenon has been interpreted within a kinetic theory by an increase of the relaxation processes on an atomic lengthscale. When the relaxation time crosses experimental timescales, the glass transition is observed.

The break in the increase of MSDs at a temperature of about 200 K was first observed by Mössbauer spectroscopy in myoglobin by Parak *et al.* (1982). Since then, it has also been observed by neutron scattering for several hydrated protein powders (cf. Section 5) and membranes (cf. Section 6), and has been interpreted by different physical models (Parak, In Press). In the two-well potential model, described in Section 4.1, the transition arises when atoms gain sufficient activation energy to explore the upper well; the process was also described in terms

https://doi.org/10.1017/S0033583502003840 Published online by Cambridge University Press

of α and β relaxation used in mode-coupling theory applied to glassy systems (Doster *et al.* 1989).

Within the framework of the two-sphere model (Bicout & Zaccai, 2001), the dynamical transition temperature is defined in an operational way as the temperature where 10% of the entire (dynamically equivalent) atomic population is in the outer, energetically higher but shallower potential, displaying larger amplitudes. Note that in both the two-sphere and the two-well model the transition is modelled by a rather smooth process, in which the MSDs gradually increase as more atoms enter the higher energy state.

4.3 Effective force constants

In order to quantify the temperature dependence of the MSDs obtained by neutron scattering, the concept of an effective force constant $\langle k' \rangle$ associated with protein resilience has been introduced by Zaccai (2000a).

$$\langle k' \rangle = 2k_{\mathrm{B}} \left(\frac{d\langle u^2 \rangle}{\mathrm{d}T} \right)^{-1}. \tag{39}$$

The effective force constant $\langle k' \rangle$ is inversely proportional to the MSDs *versus* temperature gradient. The more the MSDs increase with temperature, the less resilient or softer will be the protein. At low temperatures, in the harmonic regime $\langle k' \rangle$ corresponds to a properly defined mean force constant for a set of harmonic oscillators. Above the dynamical transition the measured $\langle k' \rangle$ value corresponds to a force constant in a quasi-harmonic approximation, or can be related to model force constants calculated in the two-well or two-sphere models (for example, Zaccai, 2000a; Bicout & Zaccai, 2001). Measured $\langle k' \rangle$ have been used in several studies to describe the rigidity of proteins and allow a quantitative comparison between different proteins in solution as well as the powder state (cf. Section 5).

5. Dynamics of hydrated protein powders

Because of the necessity to have large amounts of sample in the beam, protein dynamics was first studied by neutron scattering in 'powder' samples, non-crystalline aggregates of low water content. A justification of the biological relevance of such experiments is that a protein need not be in dilute solution but can achieve a structurally active state when surrounded by only one complete hydration layer (Rupley & Careri, 1991). One established sample preparation technique is to obtain a powder of approximately 100–200 mg of protein by lyophilization for study either in the 'dry' state or hydrated up to a few tenths of grams of water per gram of protein. In powder samples, protein translational and rotational movements can be neglected in data evaluation. Proteins that have been studied as powder samples include myoglobin, lysozyme, plastocyanin, C-phycocyanin, α-amylase, ribonuclease A, collagen, copper azurin, RNase A, superoxide dismutase (SOD) and β-lactoglobulin. Hydration values of approximately 0·4 g of water per g of protein ($h = 0{\cdot}4$ g/g) correspond to complete coverage of these small globular proteins (molecular mass $\sim$20 kDa) by one hydration shell. In general, protein powders used in neutron-scattering experiments have a maximum hydration of $h \sim 0{\cdot}5$ g/g. Protein powder dynamics has been investigated by incoherent elastic, quasielastic and inelastic scattering.

https://doi.org/10.1017/S0033583502003840 Published online by Cambridge University Press

5.1 First experiments on myoglobin

The dependence of protein function on hydration justifies the use of controlled hydration as an experimental variable during neutron-scattering experiments. The interplay of protein hydration and function has been reviewed by Rupley & Careri (1991).

In the first neutron-scattering experiments on the dynamical transition in proteins, Doster *et al.* (1989) have examined a hydrated sperm-whale myoglobin powder in an elastic temperature scan (4–350 K) with an energy resolution of 10 μeV and reported MSDs as a function of temperature using a Q-range between 1 and 5·5 $Å^{-1}$. The sample ($h = 0{\cdot}38$ g D_2O/g protein) exhibited a dynamical transition at 180 K, i.e. a deviation from the linear increase of MSD with a temperature indicative of harmonic behaviour at lower temperatures. The authors compared the protein dynamical transition to the 'glass transition' (see Section 4.2). The myoglobin data were interpreted in terms of a double-well potential for the protein H atoms (see Section 4.1). The harmonic vibrational motions were described by a Debye–Waller factor, and the excess motions above 180 K by jumps between two point sites of different energy separated by a constant distance d [cf. Eqs. (29), (30)]. Physical parameters extracted from fitting the model to the MSD values and from quasielastic scattering data were the distance $d = 1{\cdot}5 \pm 0{\cdot}1$ Å, the energy asymmetry ΔH (12 ± 2 kJ mol^{-1}) between the two sites and corresponding entropy difference $\Delta S/R = 3{\cdot}0 \pm 0{\cdot}1$. In the double-well model, all the H atoms in the protein are dynamically equivalent. Kneller & Smith (1994) have proposed an alternative interpretation of the myoglobin neutron-scattering data at temperatures above the dynamical transition. They evaluated MSDs from MD simulations obtained for liquid-like rigid-body motion of the protein side-chains, i.e. rigid side-chains undergoing continuous diffusive motions at 300 K, and showed that they fitted the experimental data quite well. They extracted diffusion coefficients according to the Einstein relation and found two linear regimes for MSDs in the time domains from 10 to 50 ps and from 50 to 150 ps with values of $1{\cdot}25 \times 10^{-7}$ and $6{\cdot}3 \times 10^{-8}$ $cm^2\ s^{-1}$, respectively.

5.2 Dynamical transitions in other proteins

Ferrand *et al.* (1993a) showed a clear dynamical transition in PMs at about 230 K, which was correlated with the onset of biological activity. The experiment is discussed in detail in Section 6.

Andreani *et al.* (1995) have used a fit of an EISF and Lorentzians [cf. Eq. (31)] in quasielastic neutron scattering (QENS) ($\Delta E = 11$–15 μeV, $0{\cdot}3\ Å^{-1} < Q < 1{\cdot}85\ Å^{-1}$) to investigate Cu,Zn SOD samples with two levels of hydration (0·25 and 0·41 g D_2O/g dry protein, respectively) in the temperature range 4–320 K. For temperatures below 200 K, the authors fitted data with the EISF alone and above that temperature with the EISF and a single Lorentzian. The experiments revealed a dynamical transition at 200 K combined with the onset of a small quasielastic component for both samples, rising to 10 and 25% contribution to total scattering at 320 K for the lowly hydrated and highly hydrated samples, respectively. The rise in MSD [determined via Eq. (29) without taking the term in brackets into account] and the quasielastic component were more pronounced for the sample with the higher hydration degree. The presence of only a small quasielastic component, whose intensity is smaller or equal to 25% of the integrated intensity, was interpreted in terms of the high structural rigidity of this predominantly β-structure protein. The authors found the linewidth of the quasielastic component of SOD to be narrower than the one for myoglobin, leading to a 20-fold increase in correlation time

https://doi.org/10.1017/S0033583502003840 Published online by Cambridge University Press

(10 ps *versus* ~0·5 ps). However, it can not be concluded that the structure is more rigid only by comparing correlation times. The variation of the jump distances (or radius) and its variation with temperature should also be taken into account. The measured MSDs of the SOD were higher than those obtained by Doster *et al.* (1989) for myoglobin at a comparable hydration degree, with a steeper gradient as a function of temperature indicating a softer structure in apparent contradiction with the quasielastic analysis.

Fitter (1999) has published a comparison of a globular water-soluble protein, α-amylase, and a membrane system, the protein–lipid complex of rhodopsin in disk membranes. Quasielastic incoherent neutron scattering ($\Delta E = 80$ μeV, $Q \sim 1$ Å^{-1}) was used to investigate samples of α-amylase in a hydrated (0·4 g D_2O/g dry protein) and dehydrated state (0·05 g D_2O/g dry protein). Disk membranes were used only in hydrated form (0·5 g D_2O/g dry membrane). The scattering data were fitted within the temperature range of 150–300 K by a sum of the EISF and two Lorentzians, representing 'slow' and 'fast' movements, respectively [cf. Eq. (31)]. In practice a broad range of relaxation times are expected in a protein giving rise to a sum of many Lorentzians, the author chose to keep two Lorentzians with linewidths of 120 μeV and 2 meV for practical reasons of fitting, with correlation times of 5·5 and 0·3 ps, respectively. Both hydrated α-amylase and rhodopsin disk membranes revealed a steep decrease of the EISF above 200 K, accompanied by an important increase of both Lorentzians with respect to the whole scattered intensity, indicating a dynamical transition near 200 K. Although both samples were found to be qualitatively similar, the hydrated membrane revealed more pronounced quasielastic components. In contrast, dehydrated α-amylase showed a steady linear decrease of the EISF over the whole temperature range as well as a steady linear increase of the quasielastic components (Fig. 2). No dynamical transition was observed in the investigated temperature range (140–300 K). Additionally, the author compared quasielastic scans performed in increasing and decreasing sample temperatures. Whereas the dry sample revealed no difference between both cycles, the wet samples exhibited a hysteresis, the quasielastic components being larger during cooling.

5.3 The role of hydration water

The experiments discussed above showed that hydration allows more complex motions to take place. Several neutron-scattering experiments have been carried out to further investigate the role of hydration water in protein dynamics.

Bellissent-Funel *et al.* (1996) examined samples of fully deuterated C-phycocyanin protein obtained from blue-green algae grown in heavy water (D_2O). The samples were equilibrated at different hydration levels ($h = 0{\cdot}1$, 0·19, 0·4 and 0·5 g H_2O/g dry protein) via vapour exchange in atmospheres of different relative humidity (RH) in H_2O. Quasielastic measurements were carried out with an energy resolution of 80 μeV and a Q-range from 0·21 to 1·28 Å^{-1} at temperatures from 273 to 313 K. The model used for data analysis was the hard-sphere potential of Volino & Dianoux (1980), [cf. Eqs. (31) and (32)]. Because of the relatively poor energy resolution, the time window of the experiment was short and slower-moving H atoms appeared immobile. Fitting immobile protein H atoms as well as strongly bound hydration shell-water molecules (within the energy resolution) with a δ function and mobile water molecules with a single Lorentzian (for high Q), $\Gamma_t(Q) = D_t Q^2/(1 + D_t Q^2 \tau_0)$, the different population fractions could be extracted, as well as the residence times τ_0 and the translational diffusion coefficient D_t. With increasing hydration degree, the fraction of the strongly bound water

https://doi.org/10.1017/S0033583502003840 Published online by Cambridge University Press

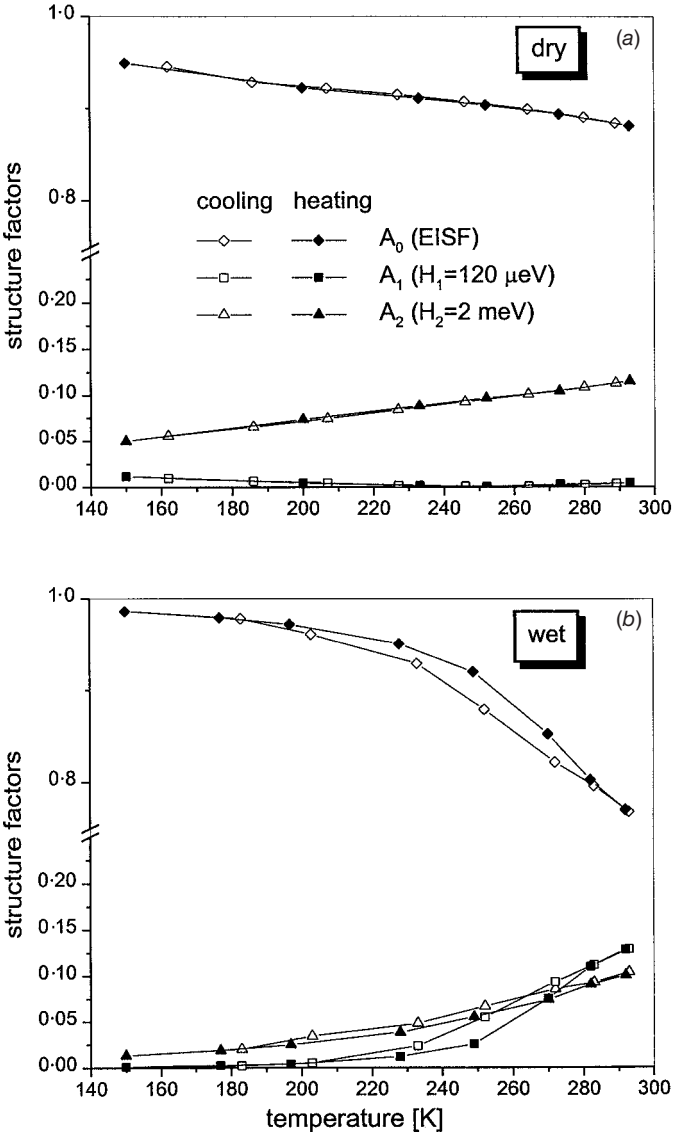


Fig. 2. The structure factor (EISF) and quasielastic components A_1 and A_2, for dry and hydrated α-amylase as a function of temperature during the heating and cooling cycle (Fitter, 1999). (Reproduced by permission of the Biophysical Society and the author.)

molecules on the protein surface was found to be strongly diminished, whereas the immobile protein protons and deuteron fraction only slightly diminished. At $h = 0{\cdot}4$ g H_2O/g dry protein, residence times of bulk and surface water were evaluated as well as diffusion coefficients for three temperatures: 273, 298 and 313 K. With increasing temperature, residence times τ_0 of surface water diminished (from 3·0 to 0·9 ps and from 8·2 to 5·9 ps, respectively) and its diffusion coefficient D_t, increased (from 0·76 to $1{\cdot}52 \times 10^{-5}$ cm^2 s^{-1} for surface water and from 1·1 to $3{\cdot}2 \times 10^{-5}$ cm^2 s^{-1} for bulk water) (Fig. 3).

Settles & Doster (1996) investigated protein-bound H_2O by excess scattering of H_2O-hydrated ($h = 0{\cdot}35$ g H_2O/g dry protein) horse myoglobin relative to a sample hydrated with

https://doi.org/10.1017/S0033583502003840 Published online by Cambridge University Press

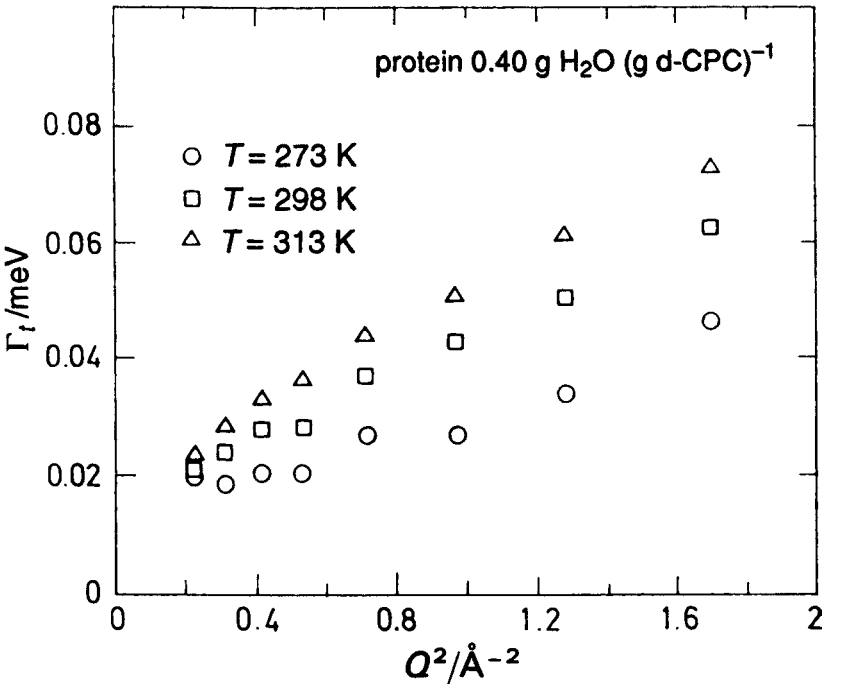


Fig. 3. Translational linewidth Γ_t of d-CPC surface water for three temperatures, 273, 298 and 313 K (Bellissent-Funel *et al.* 1996). (Reproduced by permission of The Royal Society of Chemistry.)

D_2O ($h = 0{\cdot}35$ g D_2O/g dry protein) with an energy resolution ~ 100 μeV, and $Q \sim 1$ Å^{-1}. Samples of typically 300–500 mg were obtained by re-hydrating lyophilized material with H_2O or D_2O under controlled humidity environment. Exchangeable hydrogens, making up approximately 20% of the contribution to the scattering spectra were taken into account by two limiting cases: (1) either as dynamically equivalent to water protons or (2) as non-exchangeable protons. When evaluating intermediate scattering functions of hydration water at 320 K (supposing the exchangeable protons equivalent to water protons), the authors found a Gaussian incoherent scattering function [Eq. (34)] valid for the limit $Q \rightarrow 0$. For higher Q-values, the same function was found only at short times. For longer times, the authors fitted the data with a stretched exponential KWW function [Eq. (36)] with a stretching parameter β with values between 0·3 and 0·4 indicating a deviation from the Gaussian scattering function ($\beta = 1$) (Fig. 4). With an average correlation time $\langle \tau(Q) \rangle = \int \exp(-t/\tau)^{\beta} \mathrm{d}t$, the authors extracted long time diffusion coefficients D, via Eq. (35) and in both cases found values significantly smaller than for bulk water. MSDs were obtained by a second-order polynomial fit in Q^2. The MSDs between 300 and 320 K did not follow the classical diffusion limit $\langle r^2(t) \rangle \sim t$ on a 15 ps timescale but rather a power law $\langle r^2(t) \rangle \sim t^{0{\cdot}4}$. These results were interpreted as a deviation from a homogeneous displacement of the H atoms in time and a simultaneous breaking of several hydrogen bonds.

Tarek & Tobias (2000) compared results from a MD simulation study of water-hydrated ribonuclease A with X-ray diffraction and inelastic neutron-scattering data for different temperatures. As the dynamics of protein hydration water were found to be very similar in crystal and powder environments at moderate-to-high hydration levels the authors concluded that experiments performed on powder samples are suitable for discussing hydration-water dynamics

https://doi.org/10.1017/S0033583502003840 Published online by Cambridge University Press

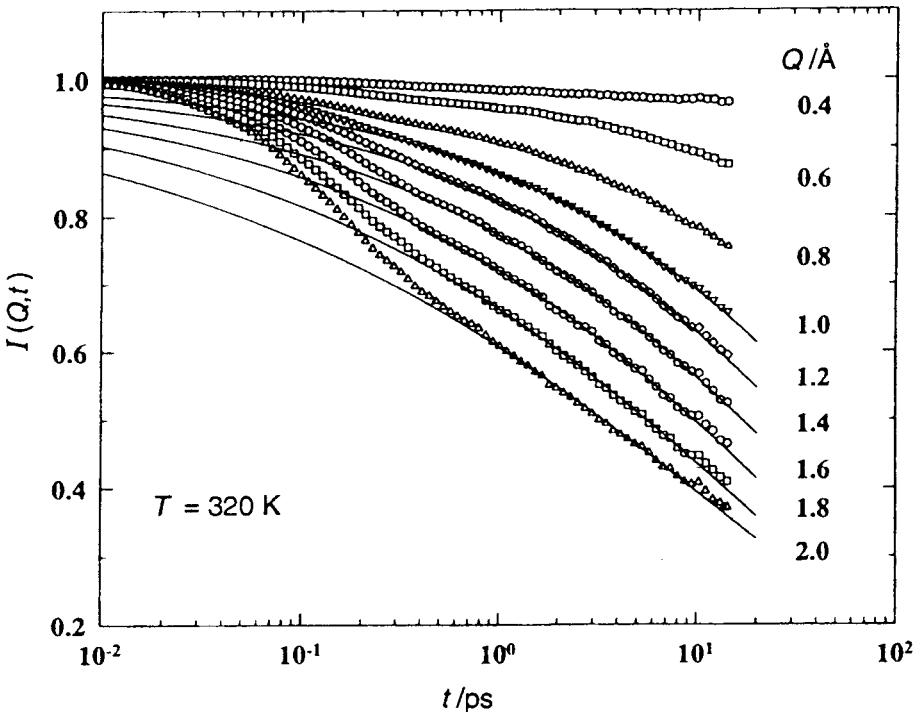


Fig. 4. Intermediate scattering function of horse myoglobin hydration water ($h = 0{\cdot}35$ g H_2O/g dry protein), assuming the exchangeable protons to be dynamically equivalent to water protons. The lines represent fits to the KWW function [Eq. (36)] (Settles & Doster, 1996). (Reproduced by permission of The Royal Society of Chemistry.)

in native protein environments. On a timescale of tens of picoseconds at room temperature and high hydration, significant water translational diffusion and rotational motions were found in the MD simulation. At low hydration, the water molecules are translationally confined but display appreciable rotational motion. Below the protein dynamical transition temperature, both translational and rotational motions of the water molecules are essentially arrested. Taken together, these results suggested that water translational motion (and not just rotation or libration) is necessary for the structural relaxation that permits anharmonic and diffusive motions in proteins.

5.4 Influence of the solvent

Several neutron-scattering experiments have been performed in recent years to investigate the influence of different solvents on the dynamical transition. Bioprotectants such as glycerol and trehalose as well as organic solvents have been used in experiments with lyophilized protein powders.

Cordone *et al.* (1999) have investigated trehalose-coated horse carbon-monoxy-myoglobin (with a ratio chosen by the authors such that 50% of the H atoms in the sample were from the sugar and 50% from the protein) by neutron scattering using elastic temperature scans (energy resolution 1 μeV and Q-range 0·43–1·93 $Å^{-1}$). Data were analysed within the Gaussian approximation [Eq. (21)]. In contrast to D_2O-hydrated myoglobin (Doster *et al.* 1989), in which a

https://doi.org/10.1017/S0033583502003840 Published online by Cambridge University Press

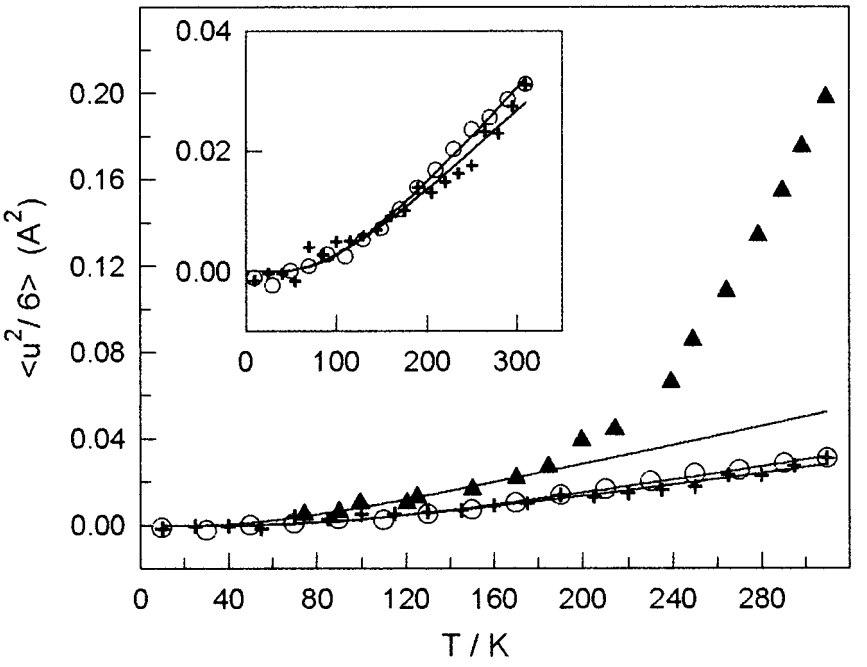


Fig. 5. MSDs of myoglobin in trehalose (○) compared to D_2O hydrated myoglobin (▲) and trehalose (+) as a function of temperature. (Reproduced from Cordone *et al.* 1999.) (Reproduced by permission of the Biophysical Society and the authors.)

dynamical transition to a non-harmonic regime has been observed at approximately 180 K, the MSDs of the trehalose-coated protein were similar to those of harmonic solids up to beyond room temperature (Fig. 5). The interpretation given by the authors was that the trehalose glass trapped the protein in a harmonic potential up to high temperatures. The quasi-harmonic behaviour was confirmed by a density-of-states measurement (see Section 5.6).

Tsai *et al.* (2000) examined the influence of glycerol on lysozyme samples. They examined lyophilized deuterium-exchanged lysozyme by elastic neutron-scattering scans ($\Delta E = 1$ μeV, Q-range from 0·25 to 1·75 $Å^{-1}$) in the temperature range from 45 K to above ambient temperature. Data were evaluated within the Gaussian approximation [Eq. (21)]. The authors prepared four samples (see Fig. 6). They found harmonic behaviour of the dry sample up to 450 K. The samples containing glycerol or water, in contrast, exhibited a dynamical transition temperature T_d, with the onset of anharmonic movements. T_d was found to be the lowest (210 K) for the sample hydrated at 0·3 g D_2O/g dry protein and was increasing with decreasing content of glycerol (270 and 330 K for the 50 and 20% glycerol samples, respectively) (Fig. 6). Dehydrated lysozyme was found to have the highest thermal denaturation temperature T_m, whereas hydrated lysozyme was found to have the lowest T_m. The T_m was decreasing with increasing content of glycerol. In the regime above T_d, larger amounts of glycerol lead to a higher rate of change in anharmonic motions as a function of temperature, rendering the material more heat labile. The authors drew the conclusion that glycerol facilitated, even though not to the same degree of water, the anharmonic transition in proteins. Below T_d, however, where harmonic motions dominate, the addition of glycerol resulted in a lower amplitude of motions.

https://doi.org/10.1017/S0033583502003840 Published online by Cambridge University Press

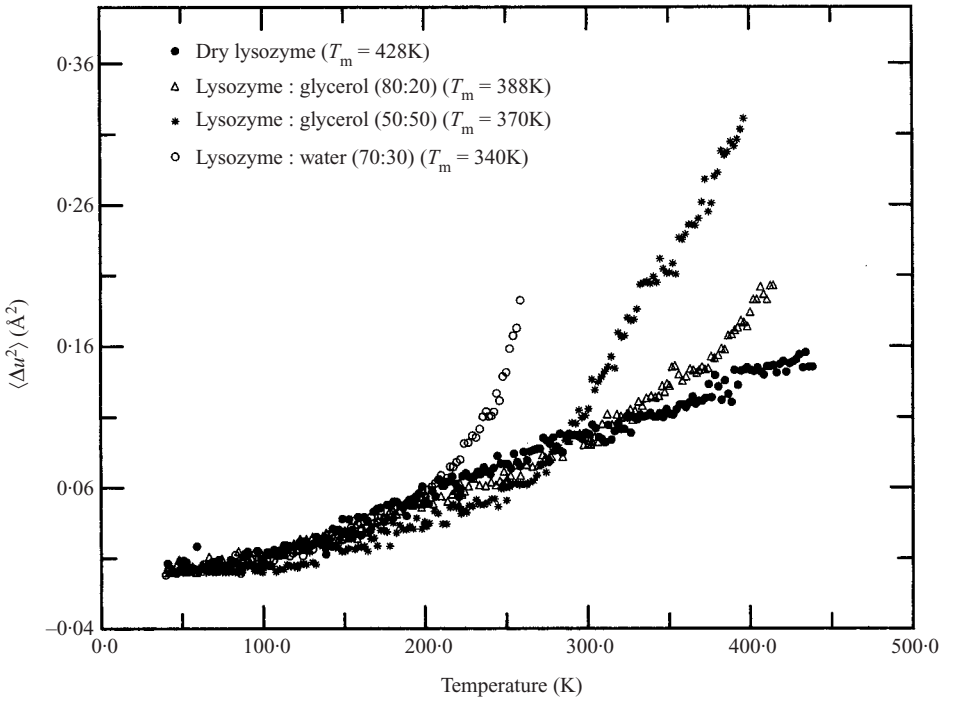


Fig. 6. MSDs of dry lysozme and lysozyme in aqueous and glycerol environments (mass ratios are given in a key on the figure) as a function of temperature. (Reproduced from Tsai *et al.* 2000.) (Reproduced by permission of the Biophysical Society and the authors.)

5.5 Diffusional motions within proteins by QENS

Tsai *et al.* (2001) compared hen egg-white lysozyme and bovine pancreas RNase A in dry and hydrated powders by elastic and quasielastic scans. The hydrated samples were washed in D_2O and submitted to vapour exchange in a D_2O atmosphere. Final hydration degrees were 0·3 g/g for the lysozyme and 0·24 g/g for the RNase. Additionally, the authors prepared a glycerol–lysozyme sample from a solution of equal amounts of glycerol and lysozyme by freeze-drying. Elastic scans were carried out between 40 and 320 K under an energy resolution of 140 μeV and a Q-range from $\sim$0·5 to $\sim$2·5 Å^{-1}. MSDs were obtained within the Gaussian approximation [Eq. (21)]. In the case of the RNase, the dry sample revealed no change in the slope of the MSDs up to the highest measured temperature whereas the hydrated sample exhibited an important increase in slope at 250 K. The fact that this temperature was more elevated than the transition temperature of myoglobin (Doster *et al.* 1989), was attributed, by the authors, to the lower hydration degree, requiring more thermal energy for the transition to occur. In addition to MSDs, the authors investigated relaxation processes via the KWW function [Eq. (36)] adding up spectra between 0·35 and 2·4 Å^{-1} for better statistics. Both dry samples could be described by a stretching exponent $\beta = 1$, over the whole temperature range, corresponding to a single relaxation process. The result was interpreted as the dry proteins being trapped in a harmonic well and only being able to exhibit vibrational modes resulting in a linear increase in MSDs with temperature. In contrast, the wet samples and the glycerol/lysozyme sample revealed a decrease of β at the transition temperature, which was more rapid and pronounced with increasing hydration. These results were interpreted by the authors as water increasing the

https://doi.org/10.1017/S0033583502003840 Published online by Cambridge University Press

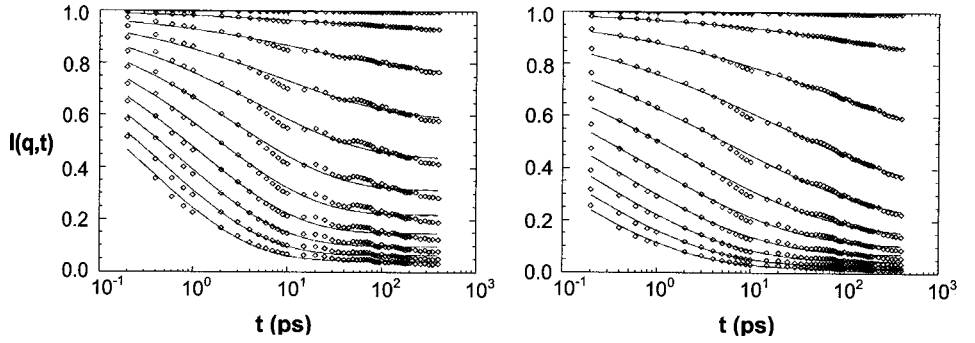


Fig. 7. Intermediate scattering function for backbone (left) and side-chain (right) atoms obtained by fitting $\Phi(t)$ in Eq. (25) by a KWW function. (Reproduced from Dellerue *et al.* 2001.) (Reproduced by permission of the Biophysical Society and the authors.)

relaxational flexibility of the protein and glycerol restricting flexibility. However, with the slope of β *versus* T being identical for glycerol at high temperatures and for the hydrated samples at low temperatures, the authors suggested that these restrictions could be overcome with sufficiently high thermal energy.

Dellerue *et al.* (2001) used QENS ($\Delta E = 96$ μeV, Q-range 0·46–1·95 Å^{-1}) on D-exchanged C-phycocyanin amorphous powder ($h = 0{\cdot}52$ g D_2O/g protein), and compared the results to MD simulations. The geometry of the atomic motions was modelled as a diffusion within spheres (adapted from Volino & Dianoux, 1980) with a distribution of radii and associated EISFs. This is certainly more realistic than a single-sphere model. The time dependence of the quasielastic component was modelled with a KWW stretched exponential law [Eq. (36)]. The time dependence of the dynamics followed stretched exponential behaviour, reflecting a distribution of relaxation times. The average side-chain and backbone dynamics were quantified and compared via their intermediate scattering functions (Fig. 7). The first dynamical parameter, β [cf. Eq. (36)], was found to be 0·4 for the protein main chain and 0·27 for the side-chains, interpreted as a wider distribution of relaxation processes of the latter. The authors used the second dynamical parameter τ, as a function of Q to address the question whether all hydrogen atoms within the sample are dynamically homogeneous or heterogeneous, corresponding to functional relationships $\tau \sim Q^{-2/\beta}$ and $\tau \sim Q^{-2}$, respectively. They found a behaviour which lay in between the extreme cases but was closer to the homogeneous case.

5.6 Inelastic neutron scattering and vibrational spectra

Since the middle of the 1990s, several papers addressed the correlation between hydration-water dynamics, protein low-frequency vibrations and the dynamical transition. After their work on the dynamical transition in myoglobin (Doster *et al.* 1989), the same group carried out inelastic scans to investigate low-frequency vibrational modes of protein dynamics (Doster *et al.* 1990). These experiments have been reviewed by Smith (1991). The density-of-states function [Eq. (27)] which is directly accessible by inelastic neutron scattering was compared by Doster *et al.* (1990) to the theoretically predicted one by the Debye model for solids. In the context of comparing experimental data with simulations, it is important to note here that the measurement relates to the sample, i.e. the protein powder, and not to a single protein.

Middendorf *et al.* (1995) measured vibrational spectra (20–4000 cm^{-1}) of dry and hydrated type-I collagen fibres (a triple-stranded helix protein which occurs in tendon, skin and bone) at

https://doi.org/10.1017/S0033583502003840 Published online by Cambridge University Press

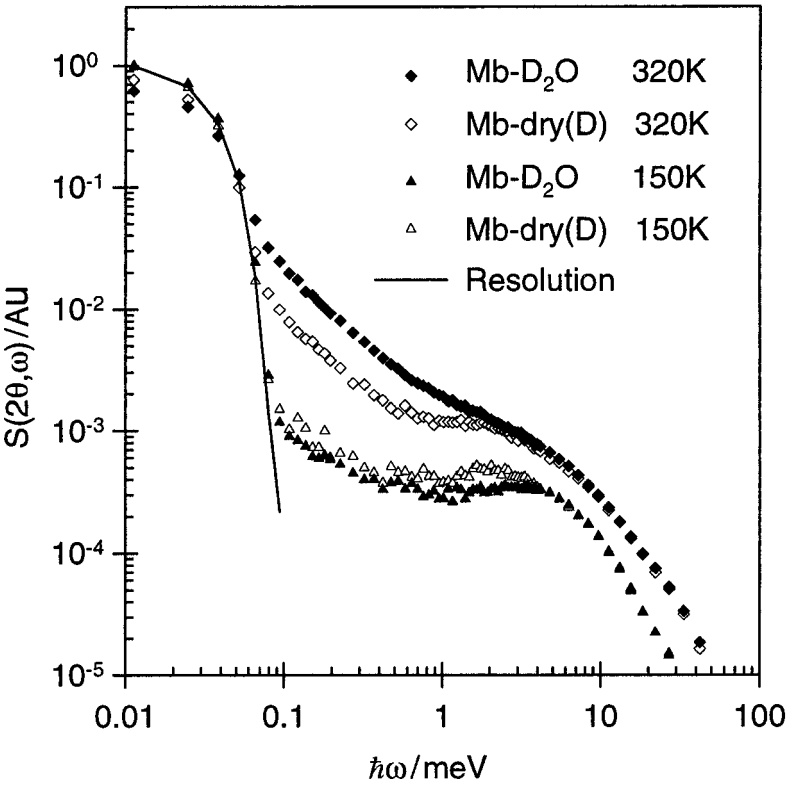


Fig. 8. $S(\mathbf{Q}, \omega)$ in arbitrary units (AU) from myoglobin in different environments at 150 and 320 K. The solid line represents the instrumental resolution. (Reproduced from Diehl *et al.* 1997.) (Reproduced by permission of the Biophysical Society and the authors.)

temperatures of 30 and 120 K. The density of states was evaluated from Eq. (27). The corresponding Q-range allowed the investigation of root MSD from 2·2 to 0·4 Å with increasing energy transfer. Hydrated samples had a water content of 0·25 g H_2O/g dry protein. A difference spectrum of dry and hydrated collagen displayed an acoustic band at 50 cm^{-1} similar to pure ice, which was assigned to phonon excitations propagating through interhelical water fractions. A second loss of scattering intensity of the dry sample with respect to the hydrated sample was present between 450 and 800 cm^{-1} reflecting the motions of protein groups hydrogen-bounded to water molecules.

Diehl *et al.* (1997) studied dry and hydrated D-exchanged horse myoglobin ($h < 0{\cdot}05$ g D_2O/g dry protein and $h = 0{\cdot}35$ g D_2O/g dry protein, respectively) as well as protonated ($h < 0{\cdot}05$ g H_2O/g dry protein) myoglobin and D-exchanged dry lysozyme using inelastic neutron scattering ($\Delta E = 30$ μeV) in the low-frequency range (below 20 cm^{-1}). The authors compared dynamic structure factors [Eq. (28)] obtained by inelastic scans of D-exchanged dry and hydrated myoglobin at 320 and 150 K. At 320 K, the hydrated samples exhibited a more pronounced quasielastic spectrum due to diffusive motions than the dehydrated samples (Fig. 8). In contrast, at 150 K, the dehydrated samples exhibit larger motional amplitudes than the hydrated ones. The excess scattering, culminating at 2 meV, was suggested to reflect water-coupled librations of polar side-chains that are depressed in the hydrated system by strong intermolecular hydrogen bonding. The same scattering excess was found for the dry lysozyme sample with

https://doi.org/10.1017/S0033583502003840 Published online by Cambridge University Press

respect to the hydrated myoglobin sample. This phenomenon was interpreted by the authors as arising from the decreased number of links of polar groups to the H-bond network when dehydrating a sample removing degeneracy and leading to modified force constants and viscous damping. According to the authors, this smaller force constant would lower the peak frequency and increase the vibrational amplitude.

Cordone *et al.* (1999) compared density-of-state functions for dry trehalose and trehalose-coated myoglobin obtained with an energy resolution of 80 μeV and a Q-range from 0·2 to 2·0 $Å^{-1}$ at 300 K. They found identical Debye behaviour ($g(\omega) \sim \omega^2$) for the two samples under 10 meV treating data according to Eq. (28). The peaks at higher energies were interpreted as vibrational modes which are not detectable in D_2O-hydrated myoglobin due to quasi-elastic scattering at ambient temperature. The authors concluded that trehalose allowed the observation of a density-of-states distribution at ambient temperatures, similar to that normally observed only at very low temperature.

Fitter (1999) measured inelastic spectra of the water-soluble protein, α-amylase and compared the results to rhodopsin-containing disk membranes via Eq. (28). The authors used an energy resolution of 80 μeV at a wavevector $Q = 1{\cdot}1$ $Å^{-1}$. The main findings were a peak (baptized 'Boson peak' in analogy to the peak observed in glass-forming systems) for the wet ($h = 0{\cdot}4$ g D_2O/g dry protein) α-amylase sample, centred at 3·8 meV (at 150 K) shifting to lower frequencies with increasing temperature. The dry α-amylase sample exhibited a less pronounced Boson peak at 2·5 meV which did not fully vanish at higher temperatures (Fig. 9). In comparison to these samples, the wet ($h = 0{\cdot}5$ g/g) disk membranes showed a Boson peak with a much broader maximum in the range 0·5–7 meV. In agreement with Diehl *et al.* (1997), the authors concluded that an increasing level of hydration shifts the peak to lower frequencies and increases its vibrational amplitudes.

Paciaroni *et al.* (1999) studied the low-frequency dynamics of copper azurin at different temperatures for a dry and D_2O hydrated sample by incoherent neutron scattering and compared experimental results with MD simulations carried out in the same temperature range. Experimental Debye–Waller factors, extracted via Eq. (28), were consistent with a dynamical transition at approximately 200 K which appeared partially suppressed in the dry sample. Inelastic and quasielastic scattering indicated that hydration water modulated both vibrational and diffusive motions. The low-temperature experimental dynamical structure factor of the hydrated protein showed an excess of inelastic scattering peaking at about 3 meV and whose position was slightly shifted downwards in the dry sample. The excess was assigned to the 'Boson peak' observed in glass-like materials. A vibrational peak reflecting the scattering by low-frequency high-amplitude modes, was reproduced by MD simulations on proteins, although at a lower energy than the observed one. The experimental quasielastic scattering of the two samples at 300 K showed a two-step relaxation behaviour with similar characteristic times, while the corresponding intensities differed only by a scale factor. Also, MD simulations confirmed the two-step diffusive trend, but the slow process seemed to be characterized by a decay faster than the experimental one. Comparison with incoherent neutron-scattering studies carried out on proteins having different structures led the authors to the conclusion that globular proteins display common elastic, quasielastic and inelastic features, with a similar hydration dependence, irrespective of their secondary and tertiary structure.

Orecchini *et al.* (2001) carried out inelastic neutron-scattering scans ($\Delta E = 30$ μeV) on dry and hydrated lyophilized β-lactoglobulin, a β-barrel globular protein, in a Q-range from 0·2 to 2·0 $Å^{-1}$ at 100, 220 and 300 K. The dynamic structure factor was extracted according to

https://doi.org/10.1017/S0033583502003840 Published online by Cambridge University Press

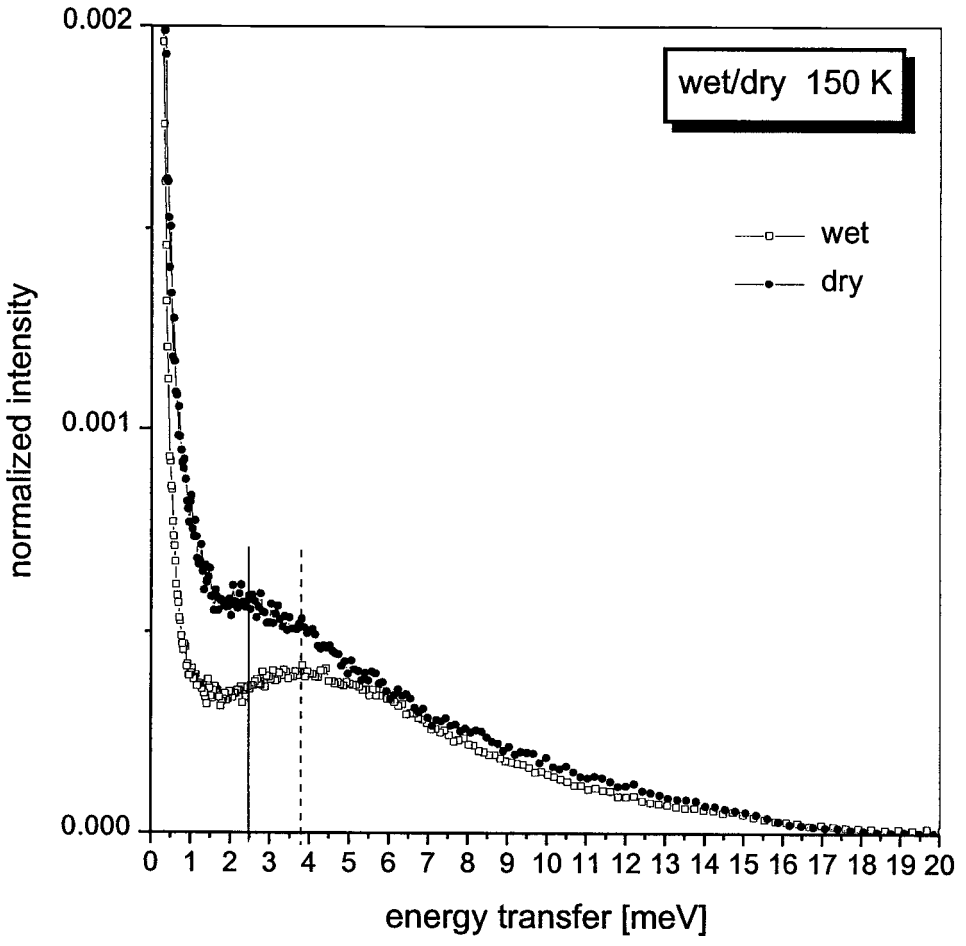


Fig. 9. The dynamical structure factor for dry and hydrated α-amylase at 150 K. The vertical lines represent the position of the scattering excesses. (Reproduced from Fitter, 1999.) (Reproduced by permission of the Biophysical Society and the author.)

Eq. (28). They investigated four samples highlighting parts by specific H_2O:D_2O exchange. Two dry samples ($h < 0{\cdot}05$ g D_2O/g dry protein) were prepared, one being protonated, the other one having its exchangeable H atoms replaced by deuterium. The two remaining samples were obtained by hydrating the first two samples at 0·4 g D_2O/g protein equilibrating them over a saturated KCl–D_2O solution. The dry sample (protonated) exhibited a scattering maximum in the inelastic region at 2·7 meV at 100 K. This maximum became less pronounced at 220 K and was completely hidden by quasielastic phenomena at 300 K. At 100 K, the maximum increased with increasing scattering vector Q (Fig. 10). An evaluation of the density of states of the dry sample at 100 K revealed a deviation from the classical Debye behaviour. An excess of states, reminiscent of the so-called boson peak in glassy systems, was found to be centred at 2·7 meV (Fig. 11). A general comparison of the dynamic structure factor of all four samples at 1·9 $Å^{-1}$ and 100 K exhibited a systematic shift of the inelastic scattering maximum to higher frequencies both for the dry protonated and dry deuterated samples with respect to their hydrated counterparts. This shift was interpreted as an increase of the force constants of the system with an increasing number of hydrogen bonds leading to higher vibrational

https://doi.org/10.1017/S0033583502003840 Published online by Cambridge University Press

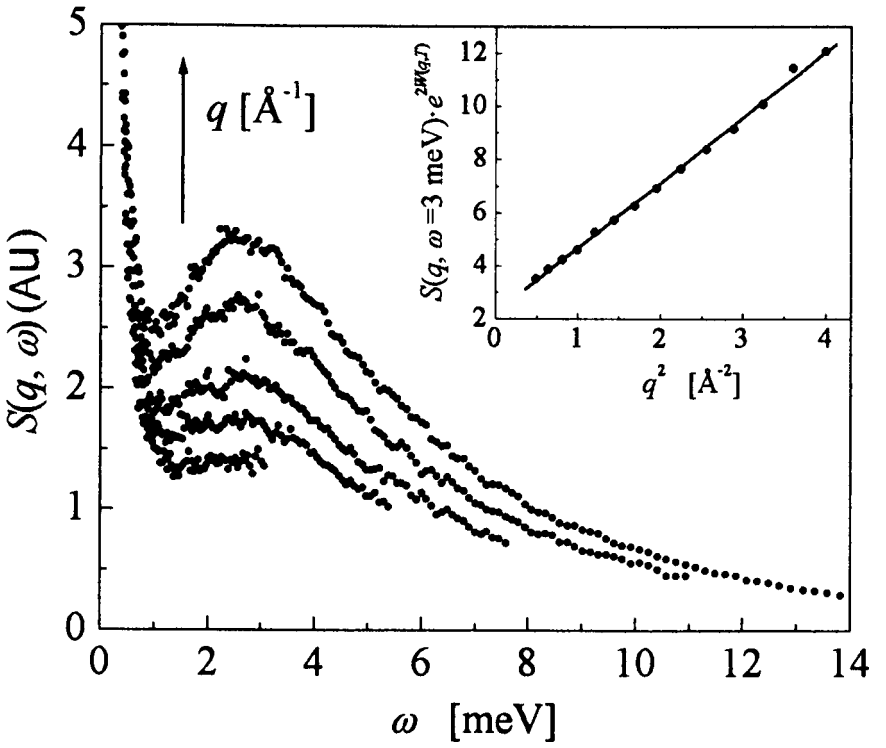


Fig. 10. Dynamic structure factor for dry β-lactoglobulin at 100 K for different values of momentum transfer: $Q = 0{\cdot}77$, $1{\cdot}02$, $1{\cdot}24$, $1{\cdot}57$ and $1{\cdot}90$ Å^{-1}, from bottom to top. (Reprinted with permission from Orecchini *et al.* 2001.) (© American Chemical Society.)

frequencies. In both D_2O-hydrated samples, the vibrations of both exchangeable and non-exchangeable protons displayed a shift towards higher frequencies. The authors concluded that the plasticizing effect of water would act over the whole protein, rather than on its surface alone.

The findings of Orecchini *et al.* (2001) were confirmed by Bizzarri *et al.* (2001) for another system. They investigated plastocyanin, an electron-transfer copper protein, by inelastic neutron scattering ($\Delta E = 60$ μeV, Q-range from $0{\cdot}4$ to $1{\cdot}8$ Å^{-1}) at 100, 220 and 300 K. They prepared two D_2O-hydrated samples ($h = 0{\cdot}4$ g D_2O/g dry protein) substituting all exchangeable hydrogen atoms in one sample and only rapidly exchanging hydrogen atoms in the other. Density of states were analysed by Eq. (28). Carrying out inelastic scans of both samples and comparing them enabled the authors to focus on the dynamic differences between exchangeable and non-exchangeable hydrogens. They found an excess of vibrational modes centred at $3{\cdot}5$ meV, similar to the Boson peak in glassy systems, which they assigned to the non-exchangeable protein protons.

5.7 Conclusions

The following general conclusions can be drawn from the experiments on protein powders, performed with various values of energy-resolution and in different Q-ranges:

(1) Protein powders (hydrated and dry) are harmonic at low temperature and behave like a Debye solid.
(2) The dynamical transition at about 180 K is more pronounced for hydrated samples.

https://doi.org/10.1017/S0033583502003840 Published online by Cambridge University Press

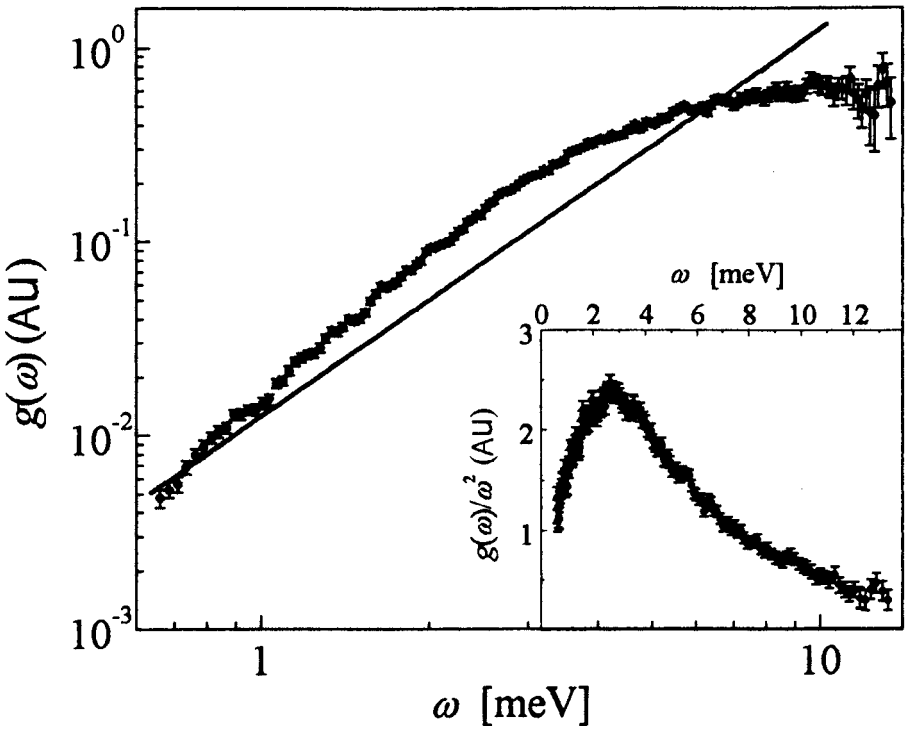


Fig. 11. Density of states of dry β-lactoglobulin at 100 K. The full line represents the Debye level. (Reprinted with permission from Orecchini *et al.* 2001.) (© American Chemical Society.)

(3) Hydration water is essential to liberate anharmonic protein motions above the transition, which are reflected in larger MSD, lower resilience, increased quasielastic scattering and a shift to lower frequencies of low-frequency vibrational modes.

The relation between protein and solvent dynamics was explored further in solution samples (see Section 7).

6. Membranes

Biological membranes are complex structures mainly made up of various protein and lipid components. In a slightly over-simplified view, the lipid component in the form of a bilayer provides the permeability barrier, while membrane spanning or associated proteins provide specific biological membrane activity such as signal transduction, selective transport, or ion pumping. Native membranes are difficult to characterize by biophysical methods because of their complexity, but considerable progress has been made through the study of membrane components separately – lipid water systems that form a wide range of polymorphic structures and membrane proteins purified and crystallized from detergent or reconstituted into lipid vesicles. The PM of *Halobacterium salinarum* is the notable exception of a natural biological membrane that has been characterized intensively by biophysical methods. It occurs naturally as a highly ordered 2D lattice made up of the light-activated proton pump bacteriorhodopsin (BR) in association with various lipids and water molecules. The dynamics of retinal rod outer-disk membranes which also contain one main protein component (rhodopsin) was discussed above in Section 5.2. The dynamics of lipid bilayers and PMs studied by neutron scattering are

https://doi.org/10.1017/S0033583502003840 Published online by Cambridge University Press

discussed in this section. Neutron-scattering studies on detergent-purified membrane proteins have been initiated (Bellissent-Funel, personal communication).

6.1 Lipid bilayers

The dynamics of L-α-dipalmitoyl phosphatidylcholine (DPPC) bilayer stacks with and without additional cholesterol molecules has been investigated by QENS in the solid (or gel) and the liquid–crystalline phases (König *et al.* 1992, 1995; Gliss *et al.* 1999). In the liquid–crystalline phase the bilayers show fluid-like membrane properties with a high molecular order of the lipid chains. Typical motions in the neutron-accessible regime are chain defects, fast head-group motions, and local diffusion of the molecule in its solvation cage (König *et al.* 1995). It has been shown that in the gel phase dynamics in DPPC can be accounted for exclusively by chain defects and that in the liquid–crystalline phase additional local diffusion of the whole molecule in its solvation cage appears (König *et al.* 1995). A high level of anisotropy in the dynamics has been found, because the molecules in the bilayer exhibit motions parallel to the normal of the membrane stack combined with locally confined motions within the bilayer plane which have been investigated separately (König *et al.* 1995; Gliss *et al.* 1999). DPPC multilayers alone exhibit displacements in the z-direction varying from 1 to 3 Å and long-range diffusion in the plane of the bilayer (König *et al.* 1992, 1995). If cholesterol is added to the bilayer the amplitude in the z-direction can rise up to 5 Å. It has been suggested that at higher temperatures ($T \geqslant 36\ ^{\circ}\mathrm{C}$) cholesterol can move between the opposite leaflets of the bilayer and the in-plane motion is dominated by discrete, large-angle rotational jumps of the steroid body (Gliss *et al.* 1999). The lipid dynamics in multilayers is strongly influenced by the lipid-packing density, which has already been seen with lateral diffusion. One way to change the packing density is by varying of the degree of hydration of the multilayers (Levine *et al.* 1968; König *et al.* 1995). The packing density is increased by lowering hydration and it has been suggested that the packing density plays a major role for the dynamic behaviour of the lipids (König *et al.* 1995).

6.2 BR and the purple membrane (PM)

BR is a retinal-binding protein that functions as a light-activated proton pump. A photocycle of retinal colour changes is associated with its activity. BR is organized with lipids in a 2D lattice, forming the PM. This membrane, which is a part of the cell membrane of *Halobacterium salinarum*, an extreme halophilic archaeon, can easily be isolated from the organism and is extremely stable. The relationship between structure, hydration and dynamics, on one hand, and BR activity, on the other, has been explored by neutron-scattering studies of PM. A protein is only active if it adopts its specific 3D structure and also if all the internal motions necessary to its function can be accomplished. Based on this dynamics–structure–function relation, Zaccai (1987) has suggested a hypothesis that the inhibition of BR activity at low temperatures or in the dry state would be due to an inhibition of motions by the close packing of lipids around the protein in PM. Neutron experiments on the PM have been reviewed by Zaccai (2000b).

6.2.1 The dynamical transition in the PM

A first set of incoherent neutron-scattering experiments (elastic temperature scans with $\Delta E \sim 8\ \mu\mathrm{eV}$ in a Q-range from 0·3 to 5·5 $\mathrm{Å}^{-1}$) supporting the hypothesis in the previous paragraph has been performed on two extreme hydration states of PM (dry at 0% RH and

https://doi.org/10.1017/S0033583502003840 Published online by Cambridge University Press

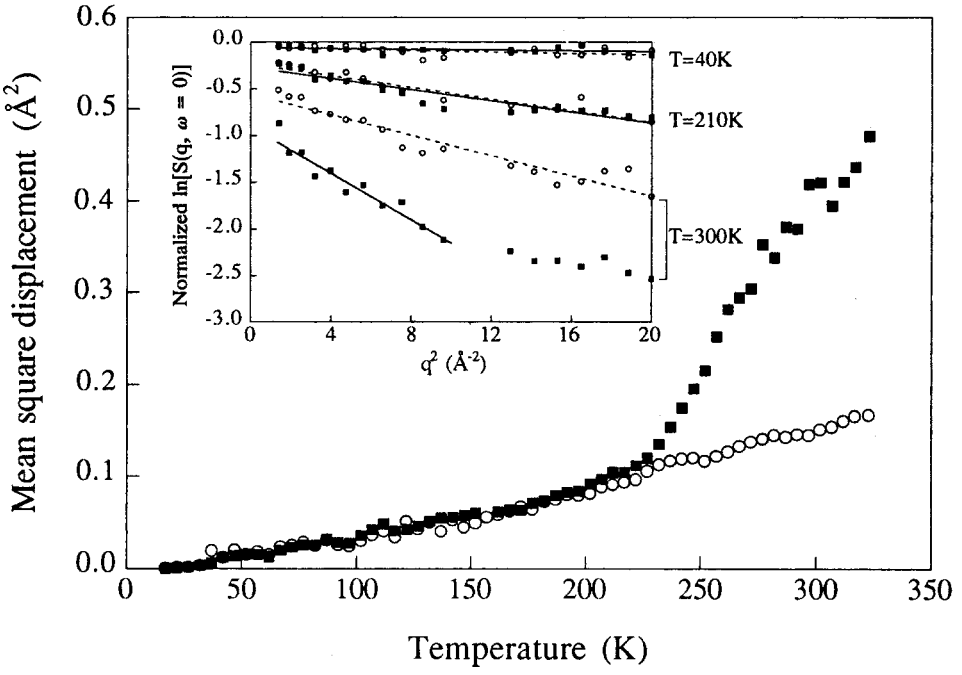


Fig. 12. MSDs as a function of temperature of dry and hydrated (0·55 g H_2O/g dry membrane) PM obtained within the Gaussian approximation. The increase of the slope for MSDs of the dry sample is about 10^{-3} Å^2 K^{-1}. (Reproduced from Ferrand *et al.* 1993a.) (© National Academy of Sciences, USA.)

hydrated at 93% RH, respectively) (Ferrand *et al.* 1993a, b). A dynamical transition at approximately 230 K between harmonic and non-harmonic motions was observed only for the hydrated PM sample (Fig. 12). Below this temperature the hydrated sample, following a harmonic behaviour, is not active, whereas above the transition temperature non-harmonic diffusive motions appear and the BR photocycle can be completed. In contrast to this, the dry PM sample exhibits harmonic motions up to room temperature and BR is not functional in the entire temperature range. The fact that non-harmonic motions are not necessarily liberated at high temperatures indicates that temperature alone is not sufficient to obtain high amplitudes of motion. These results significantly support the hypothesis that a global soft environment obtained through temperature and hydration, which allows larger diffusive thermal motions, is required to ensure the protein activity. Complementary studies of the elastic incoherent scattering for smaller scattering vectors have demonstrated a dynamical transition at approximately 150 K, which is present for both the dry and the hydrated membrane (Réat *et al.* 1997). This has led to a division of PM dynamics into two different categories of motions: the 'high' amplitude motions exhibiting smaller frequency and higher amplitude motions, which achieve a maximum of 2 Å^2 at 300 K for the hydrated PM sample, and a population of 'small' amplitude motions at a higher frequency and smaller amplitudes up to values of 1 Å^2.

6.2.2 QENS from oriented PM

A different approach using quasielastic incoherent neutron scattering on oriented PM samples has yielded information about the diffusive motions of different spatial extent and with different correlation times in the nano- to picosecond timescale (Lechner *et al.* 1992; Fitter *et al.* 1996a).

https://doi.org/10.1017/S0033583502003840 Published online by Cambridge University Press

This technique has allowed characterization of the main components of diffusive motions such as three-site jump diffusion of methyl group rotations and two-site jump diffusion (Lechner *et al.* 1992; Fitter *et al.* 1996a). The onset of quasielastic scattering has been found around 200 K with a particular strong increase of this component around 260 K (Fitter *et al.* 1996c). Moreover, the different categories of diffusive motion have been found to depend on the hydration state of PM (Fitter *et al.* 1996a), supporting the hypothesis that a decrease in hydration results in a solidification in internal molecular flexibility of the protein structure. It has been concluded that the observed diffusive motions are essential for BR photocycle activity. The role of the lipid environment on PM dynamics has been characterized by using partly delipidated PM samples, which are still crystalline and arranged as BR trimers (Fitter *et al.* 1998b). A reduced flexibility of the membrane has been observed, which was more pronounced for the wet than for a dry membrane. This has led the authors to the conclusion that it is the hydration of the lipids which plays a major role with respect to the dynamical properties of the protein–lipid complex (Fitter *et al.* 1996b) as suggested by Zaccai (1987). A comparison between PM and disk membranes, which contain the protein rhodopsin and lipids with a higher lipid weight ratio compared to the one of PM, has indicated a higher internal flexibility of the disk membranes (Fitter *et al.* 1998a). The results have been interpreted in the context that the increase of lipid–protein ratio in the membrane mainly influences the dynamical behaviour. However, such an interpretation should be made with caution because the rhodopsin structure has larger extramembrane loops than BR, which may result in an increased internal flexibility of the molecule.

6.2.3 Hydration dependence of PM motions

The hydration dependence of the thermal motions has been investigated further in a broad temperature range (Fitter *et al.* 1997; Lehnert *et al.* 1998). 'Fast' and 'slow' motions as defined by the correlation time from quasielastic measurements have been shown to be influenced differently by hydration. In general, the slower local diffusive motions become much more pronounced at a high hydration state, which led to the suggestion that they correspond to motions of groups close to the surface of the membrane (Fitter *et al.* 1997). The behaviour of the $\langle u^2 \rangle$ values, as a function of temperature upon hydration changes, has shown that the two populations of high- and small-amplitude motions respond differently to hydration of the membrane (Lehnert *et al.* 1998) (Fig. 13). These results have quantified the dynamical heterogeneity of the membrane and its dependence on hydration and temperature. The high-amplitude motions in the non-harmonic region above the transition at 250 K are not very sensitive to changes in hydration until a high state is achieved where a sharp increase of the $\langle u^2 \rangle$ values is seen. In contrast to this, the small-amplitude motions above the transition temperature rise continuously with hydration. From the hydration dependence of photocycle and pumping characteristics of BR a correlation has been made to the thermal motions. It has been shown that not only is a global fluidity necessary for the functioning of BR, but that the particular response to hydration of the different populations of motions can be correlated to the functional behaviour of BR. The examination of the lamellar spacing of PM stacks as a function of temperature by neutron diffraction has shown that cooling of a PM sample leads to a decrease in the lamellar spacing (Lechner *et al.* 1998). The authors suggested that this corresponds to dehydration of PM that takes place around 270 K. Upon heating this effect is reversible and rehydration starts around 255 K. The initial spacing is reached again at about 275 K. This process has been put in context with the dynamical behaviour and the transition temperatures of the

https://doi.org/10.1017/S0033583502003840 Published online by Cambridge University Press

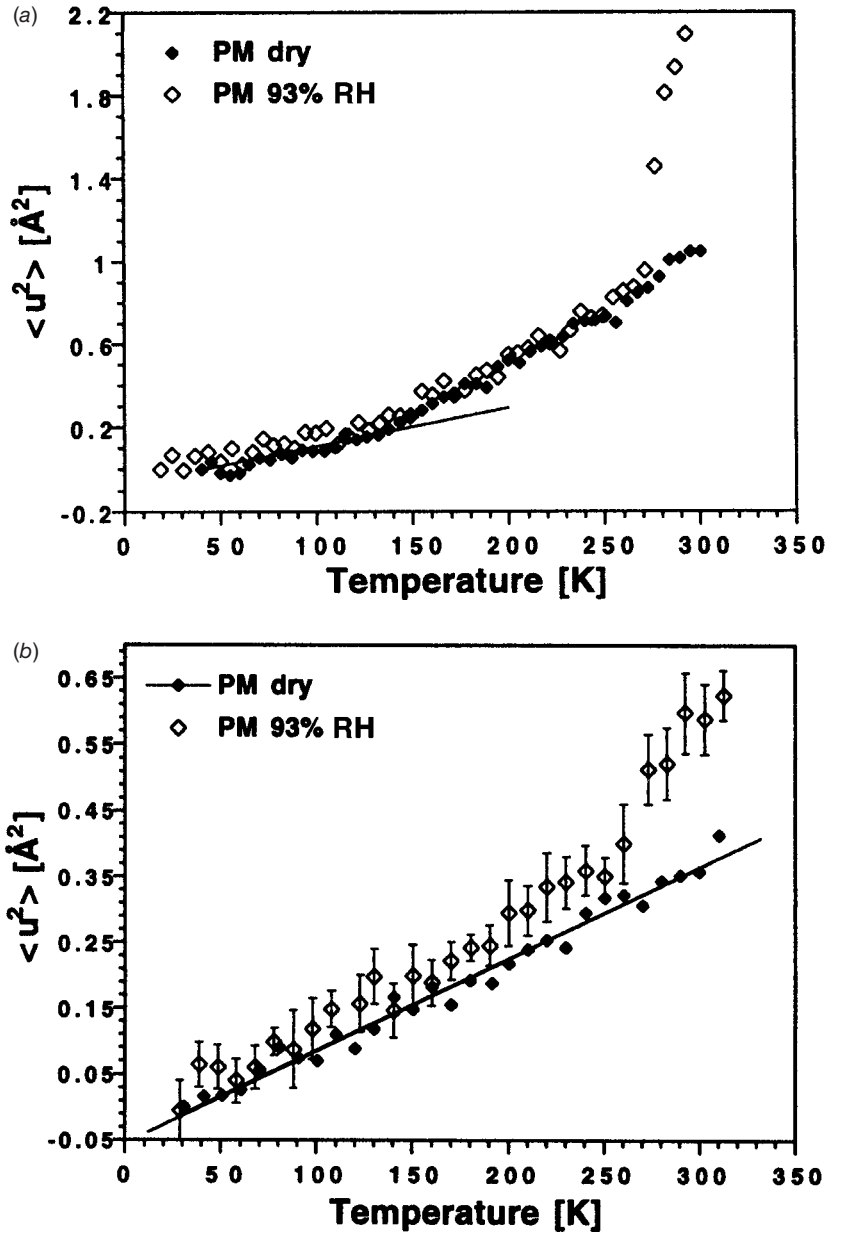


Fig. 13. MSDs of hydrated PM from two different fit ranges: (*a*) 0·3 $Å^{-1} < Q < 1·8$ $Å^{-1}$ (low Q-range) and (*b*) from 2·04 to 3·6 $Å^{-1}$ (high Q-range). (Reproduced from Lehnert *et al.* 1998.) (Reproduced by permission of the Biophysical Society and the authors.)

membranes. In particular, the rehydration starting around 255 K has been correlated to the transition temperature around 250 K and the solvent melting effect observed by Réat *et al.* (1997).

6.2.4 Local dynamics in PM studied by isotope labelling

Local dynamics of the protein core have elucidated the dynamical heterogeneity of BR in more detail (Réat *et al.* 1998). For this purpose a completely deuterated membrane with

https://doi.org/10.1017/S0033583502003840 Published online by Cambridge University Press

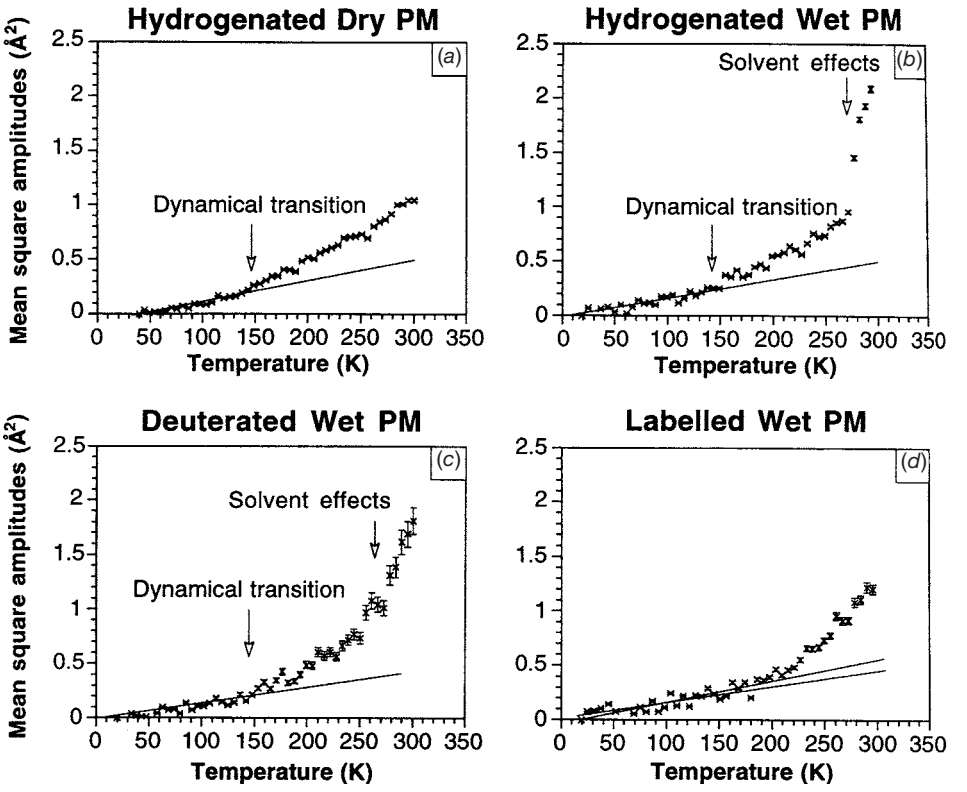


Fig. 14. MSDs for different PM samples as a function of temperature. The labelled sample is a deuterated membrane with hydrogenated retinal and two amino-acid types. Dry samples are at 0·02 g D_2O/g dry protein, wet samples at 0·45 g D_2O/g dry membrane (deuterated labelled sample) and at 0·55 g D_2O/g dry membrane (hydrogenated PM). (Reproduced from Réat *et al.* 1998.) (© National Academy of Sciences, USA.)

hydrogenated retinal – that is the light-sensitive chromophore of BR – and two different amino-acid types have been prepared. These selected groups cluster in the functional centre of the protein and are located in the retinal-binding pocket and the extracellular moiety of BR. The mean square amplitudes $\langle u^2 \rangle$, of a hydrated, labelled PM sample show significantly decreased flexibility compared to the global membrane, with the motions revealed as being more restrained and shielded from solvent melting effects (Fig. 14). These results have been interpreted in terms of a more rigid protein core, which is required to ensure uni-directional proton transfer across the membrane and to control stereo-specific selection of retinal conformations. The retinal-binding pocket has to act as a valve between the extracellular and cytoplasmic parts of BR, and therefore a certain environmental rigidity is required, whilst in the meantime large conformational changes have to be accomplished, which need a global fluidity of the membrane.

6.2.5 Dynamics of different BR conformations

The dynamical behaviour of a BR mutant (D96N), which can be trapped in two different conformations, has been investigated. Despite important structural differences between the two conformations no change in dynamics has been stated (Fitter *et al.* 1999).

https://doi.org/10.1017/S0033583502003840 Published online by Cambridge University Press

7. Protein solutions

7.1 From powders to solutions

Most early neutron-scattering experiments dealing with protein dynamics have been carried out on protein powders. The difficulties that had to be resolved in treating data from protein solutions arise from having to correct for solvent scattering and for translational and rotational diffusion of the protein particles in order to focus on internal protein dynamics.

Hydration plays a determinant role for protein activity, stability and dynamics. The most impressive effect of water is certainly its influence on the onset of activity of several enzymes at approximately 0·2 g H_2O/g protein whereas they remain inactive at lower levels of hydration (Rupley & Careri, 1991). Many experiments have been performed to study the effect of hydration on small enzymes (Rupley *et al.* 1983), and it is interesting to note that there are different definitions of full hydration. For example, full hydration has been defined as the level above which the specific heat capacity of protein remains constant (Yang & Rupley, 1979) or as the hydration level below which no ice formation occurs (Kuntz & Kanzmann, 1974).

Hydration effects on protein dynamics have been studied by neutron scattering mainly on hydrated powders (see Section 5). Recently, however, careful experiments were performed in solution. Using IQNS, Pérez *et al.* (1999) compared myoglobin and lysozyme picosecond internal dynamics in D_2O solution to that in hydrated powders by quasielastic incoherent neutron scattering ($\Delta E \approx 70$ μeV, $0{\cdot}3\ \text{Å}^{-1} < Q < 2{\cdot}0\ \text{Å}^{-1}$). Pérez *et al.* (1999) found that from dry powder to coverage by one water layer, the surface side-chains progressively acquired the ability to diffuse locally. At higher hydration levels, the main effect of water was to increase the rate of these diffusive motions. Motions with higher average amplitude occurred in solution, about three times higher than for a hydrated powder at complete coverage, with a shorter average relaxation time, approximately 4·5 ps compared to 9·4 ps for one water monolayer. It was found for several globular proteins that the heat capacity does not change upon hydration after complete coverage of protein by water, which occurs at around 0·4 g D_2O/g protein. However, this is not inconsistent with higher diffusion of surface side-chains with increasing hydration, because these motions do not necessarily break or create new hydrogen bonds.

Zaccai *et al.* (2000) compared the MSD of proteins in D_2O solution and in D_2O-hydrated powders and showed that, at the protein concentration used (100–200 mg ml^{-1}) in the solution, the $\langle u^2 \rangle$ values were shifted to higher values with respect to the values from the powder sample. On the other hand, the slope of $\langle u^2 \rangle$ *versus* T (in the restricted temperature range in which the solution could be studied, 280–320 K) was the same for the solution and the powder.

The neutron-scattering experiments in solution described above have been performed in D_2O, to reduce the scattering contribution of the solvent. However, D_2O has important effects on protein stability and solubility (Némethy & Scheraga, 1964; Bonneté *et al.* 1994), so that observations made in D_2O solutions cannot be assumed to reflect behaviour in H_2O (see Section 3.3). Tehei *et al.* (2001) measured protein dynamics by incoherent elastic neutron scattering in H_2O solutions. Because bulk solvent and protein motions are in different space–time windows, by using a IN13 backscattering spectrometer where the space–time window corresponds to approximately 1 Å in 0·1 ns, bulk water diffusive motions corresponding to a $\langle u^2 \rangle$ value of about 100 Å^2 in 0·1 ns, were filtered out in practice because they were well outside the measurement window (see Section 3.1).

https://doi.org/10.1017/S0033583502003840 Published online by Cambridge University Press

7.2 Water dynamics and solvent dependence of the dynamical transition in proteins

Although the behaviour of pure bulk water is not within the scope of this review, it is of interest to briefly summarize characteristic changes in water structure and dynamics at cryo-temperatures in order to appreciate their possible influence on protein dynamics.

Water can be in a supercooled, liquid state at temperatures below 0 °C if crystallization is prevented, but necessarily crystallizes into ordinary hexagonal ice if the temperature approaches 235 K, the point of homogeneous nucleation at atmospheric pressure (Kanno *et al.* 1975). In contrast, if the temperature is rapidly lowered to, for example, liquid-nitrogen temperature (77 K) – that is flash-cooling – amorphous ice is formed (for a review on glass formation of liquids see Angell, 1995; Debenedetti & Stillinger, 2001). Amorphous bulk water undergoes a glass transition upon heating to 136 K (McMillan & Los, 1965; Johari *et al.* 1987; for a review see Mishima & Stanley, 1998). At temperatures around the glass transition, water molecules gain rotational mobility (Fisher & Devlin, 1995). At 150–155 K, evidence has been presented for translational diffusion to occur concomitant with crystallization (Smith & Kay, 1999). The glass transition of water increases above 136 K if, for example, organic solvent or salt are added or if water is confined.

Does the solvent glass transition trigger a dynamical transition in the protein? In other words, is protein dynamics enslaved to solvent dynamics (Iben *et al.* 1989)? Réat *et al.* (2000) addressed this issue by performing neutron-scattering experiments on IN6 (energy resolution 50 μeV) using xylanase in pure D_2O and in various cryo-solvents characterized by different glass transition temperatures. Dynamical transitions of picosecond motions in the protein were determined. The dynamical behaviour of the protein was found to largely follow that of the surrounding solvent. In pure D_2O, a sharp dynamical transition ($\sim$270 K) was observed close to the melting temperature of water. In mixed solvents, the protein exhibited a dynamical transition at $\sim$230 K, a temperature close to the glass transitions of all but one of the solvents studied (70% CD_3OD/30% D_2O). The glass transition at 190 K in 70% CD_3OD/30% D_2O was thus proposed to be decoupled from the picosecond dynamic transition behaviour of the protein, yet possibly coupled to slower motions. This is in line with a study of stacked PM separated by layers of amorphous water that revealed a glass transition of inter-membrane water at least 30 K below the picosecond dynamical transition of the membrane (Weik *et al.*, unpublished observations). In view of their diverse results, Réat *et al.* (2000) suggested that the onset of anharmonic protein motions takes place at a temperature that is determined either by the protein or the solvent, depending on which component has the higher transition temperature.

How the observed values of dynamical transition temperatures vary with instrumental resolution has been addressed by Daniel *et al.* (1999). These authors performed neutron-scattering experiments on the enzyme glutamate dehydrogenase (GDH) in a cryo-solution at two spectrometers at the ILL, with different energy resolution. IN16 and IN6 are characterized by an energy resolution of 1 and 50 μeV, respectively. Therefore, motions faster than 5 ns on IN16 and faster than 100 ps on IN6 contribute to the measured MSD. The onset of anharmonicity for nanosecond motions (IN16) has been shown to take place at $\sim$140 K, whereas in the picosecond timescale (IN6), the dynamical transition was observed at $\sim$220 K. The onset of anharmonic motions takes place at a lower temperature for the slower motions.

8. Comparing neutron scattering with other techniques

The dynamical transition was first seen in myoglobin by Mössbauer spectroscopy (Parak *et al.* 1982, and reviewed by Parak, In Press) and the reduction of protein-specific motions when

https://doi.org/10.1017/S0033583502003840 Published online by Cambridge University Press

myoglobin is embedded in a trehalose glass (see Section 5.4) was first observed by optical absorption spectroscopy (Cordone *et al.* 1998).

Melchers *et al.* (1996) compared Raman, Mössbauer and optical absorption spectroscopy results on myoglobin with normal mode calculations. Each of the techniques is sensitive to different aspects of protein dynamics; the MSDs of the iron atom measured by Mössbauer spectroscopy were used to probe the overall motion of the haem within the protein matrix whereas the thermal line-broadening of the Soret band and the resonance Raman bands were used to detect local intramolecular iron–porphyrin motions.

The influence of hydration on the internal dynamics of a typical EF-hand calciprotein, parvalbumin, was investigated by solid-state ^{13}C-NMR spectroscopy and incoherent quasi-elastic neutron scattering using the powdered protein at different hydration levels. Both approaches establish an increase in protein dynamics upon progressive hydration above a threshold that only corresponds to partial coverage of the protein surface by the water molecules (Zanotti *et al.* 1999).

Bon and collaborators (Bon *et al.* 1999, 2002) performed neutron studies on the structure and dynamics of protein-hydration water at room temperature using protein crystals of hen egg-white lysozyme. Neutron crystallography revealed that 80% of the water molecules belonging to the solvent part of the crystal are either fully ordered or partly disordered and form a first hydration shell. The remaining 20% are fully disordered, cannot be identified in the density maps and are part of an incomplete second hydration shell (Bon *et al.* 1999). QENS experiments revealed that 75% of the protons assigned to the solvent part of the crystals undergo long-range translational jump diffusion, with a diffusion coefficient reduced by five- to six-fold compared to bulk water (Bon *et al.* 2002). Twenty-five per cent of the solvent protons showed pure translational (as opposed to jump) diffusion with a diffusion coefficient reduced by 50-fold compared to bulk water. Combining the structural and dynamical results, it has been concluded that water molecules belonging to the first hydration shell occupy reasonably well-defined hydration sites and form a tight, yet mobile and rapidly exchanging hydrogen-bonding network. Beyond these, water molecules of the second hydration shell do not occupy well-defined positions and are considerably less mobile.

9. Biological relevance

9.1 Dynamics–activity relations

Dynamics–activity relations have been studied by neutron scattering in considerable detail in PMs (see Section 6.2).

9.2 Dynamics–stability relations (adaptation to extreme environments)

Thermophilic organisms grow optimally at temperatures above 60–70 °C (Adams & Kelly, 1995; Madigan & Marrs, 1997), psychrophiles grow in polar waters at temperatures just above freezing (Arnold *et al.* 2001), while halophiles grow only in hypersaline environments, salt lakes like the Dead Sea or salt marshes (Mevarech & Neumann, 1977; Oren, 1986). The stability and catalytic activity of proteins are well-known to be highly affected by temperature and solvent salt concentrations and most proteins from mesophilic organisms are denatured at high temperatures and precipitate in high salt. If a cell can live and divide under such extreme

https://doi.org/10.1017/S0033583502003840 Published online by Cambridge University Press

conditions, then it follows that its proteins are folded and functional, i.e. stable and active. What are the molecular mechanisms involved in adaptation to extreme environments?

It has been assumed that increased structural rigidity preserves the specific fold of a thermophilic protein structure at high temperatures (Jaenicke, 2000), while proteins from psychrophiles display higher internal conformational flexibility required for appropriate activity at low temperature (Arnold *et al.* 2001). However, stability need not necessarily be associated with lower flexibility. By comparing a mesophilic α-amylase with its thermophilic homologue, Fitter & Heberle (2000) and Fitter *et al.* (2001) investigated the relationship between thermal stability and internal equilibrium fluctuations. IQNS in the picosecond time range ($\Delta E \approx 100$ μeV, $Q_{max} = 2{\cdot}25$ Å^{-1}) were used to study dynamic features of the folded state of each protein at room temperature. The data revealed larger fluctuation amplitudes for the thermophilic α-amylase, suggesting higher conformational freedom for this enzyme compared to its mesophilic homologue. Entropic stabilization was the proposed mechanism for increased thermal stability in this case. However, experiments were performed in D_2O solvent, which is known to influence protein stability (see Section 3.3) and the extrapolation of the neutron-scattering results to physiological conditions may not be justified. Energy-resolved elastic incoherent neutron-scattering experiments ($\Delta E = 8$ μeV, $Q \sim 1$ Å^{-1}) on bovine serum albumin in H_2O and D_2O solution respectively, showed that the higher thermostability of the protein in D_2O is associated with lower rigidity, i.e. entropic fluctuations. It would be of great interest to repeat the experiments on the mesophilic and thermophilic α-amylases in H_2O solution.

The relation between stability and dynamics was also studied by neutron scattering in a protein from an extreme halophile. Halophilic malate dehydrogenase from *Haloarcula marismortui* (*Hm*MalDH) itself requires molar salt in order to be stable and soluble. It has been studied extensively and has different stability behaviour in H_2O and D_2O solutions containing molar concentrations of either NaCl or KCl. Energy-resolved elastic incoherent neutron-scattering experiments were performed with $\Delta E = 8$ μeV in the Q-range ~ 1 Å^{-1}. They provided values of mean-squared atomic fluctuations on the 0·1 nanosecond timescale. Effective force constants, characterizing the rigidity of the protein structure, were calculated from the variation of the mean squared fluctuation with temperature. The rigidity of *Hm*MalDH increased progressively with increasing stability, from molar NaCl in H_2O, via molar KCl in D_2O to molar NaCl in D_2O. The higher stability is associated with increased rigidity showing the dominance of enthalpic terms arising from bonded interactions (Fig. 15). From previous data it was suggested that these are associated with hydrated ion binding stabilizing the protein in the high-salt solvent (Tehei *et al.* 2001).

9.3 Protein folding

Besides structural and thermodynamic studies, dynamic information is also necessary to gain insight into the mechanisms of protein folding. Protein dynamics experiments can provide information on the shape of the energy surface explored by a protein at different stages in folding, including partially folded and denatured states. The rate of protein folding is determined by both the energy landscape and by the protein dynamics (Karplus & Weaver, 1994; Burton *et al.* 1998; Chan & Dill, 1998; Portman *et al.* 2001). While the energy landscape of protein folding has been the subject of intense study, little is know experimentally about the dynamic behaviour of a denatured protein. Such dynamic experiments can help us learn the physics and

https://doi.org/10.1017/S0033583502003840 Published online by Cambridge University Press

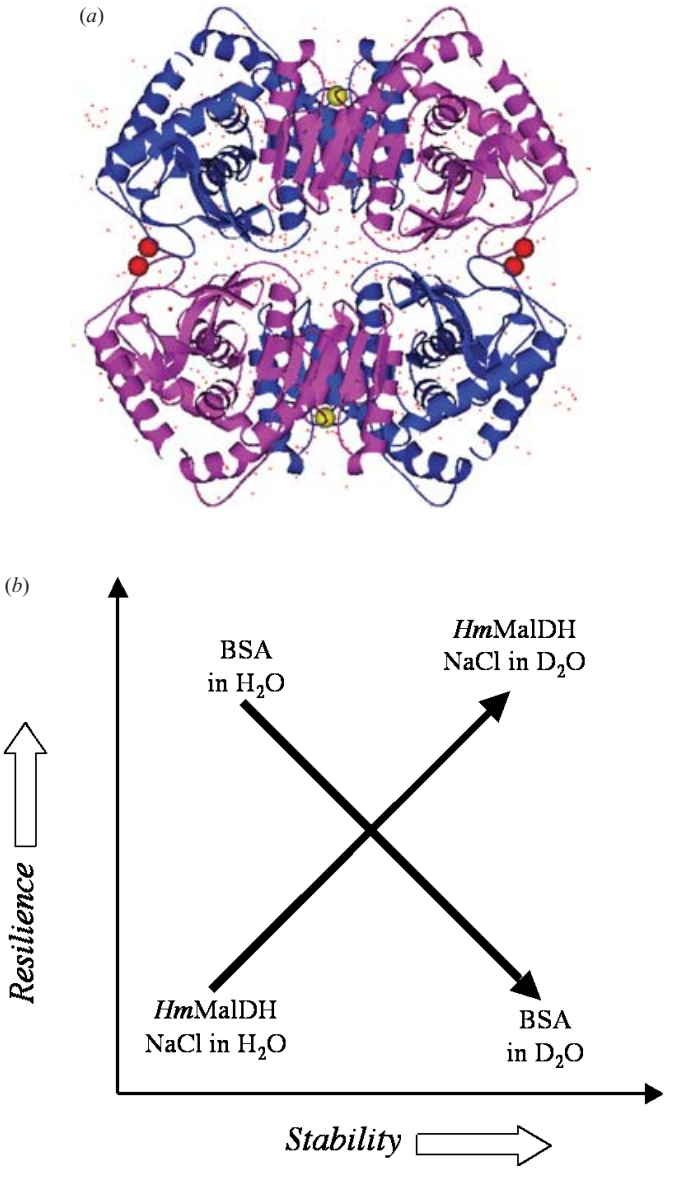


Fig. 15. Dynamics and stability of halophilic malate dehydrogenase. (*a*) The structure of halophilic malate dehydrogenase showing bound solvent (yellow balls, sodium; red balls, chloride; red dots, water molecules). (*b*) Schematic diagram relating resilience and stability in different solvents for *Hm*MalDH and BSA. Enthalpy-driven stabilization leads to greater resilience while entropy-driven stabilization leads to lower resilience.

chemistry principles that govern protein folding. In addition to their roles as protein folding intermediates, partially folded proteins have also been shown to be important in cell functions (Wright & Dyson, 1999). Certain partly ordered protein conformations, commonly called molten globule states exhibit a high content of native-like secondary structure, considerable compactness, but lack the extensive, specific side-chain packing interactions of a native structure (Ptitsyn, 1995). Structural studies have shown that the side-chains in a molten globule are more

https://doi.org/10.1017/S0033583502003840 Published online by Cambridge University Press

disordered and can adopt a greater variety of conformations than in a native protein (Doig & Sternberg, 1995; Klefhaber *et al.* 1995).

Neutron scattering offers a method to study the dynamics, with the advantage of measuring motions on different time- and lengthscales. First incoherent quasielastic neutron-scattering experiments of the dynamics of a denatured protein were performed on yeast phosphoglycerate kinase (Receveur *et al.* 1997). Using a model of diffusion in a sphere of radius *a*, these experiments revealed a change in the fast (picosecond timescale) diffusive internal dynamics of the protein. The diffusing fraction changed, from approximately 60% in the native protein to approximately 82% in the denatured protein. The radius of the sphere also changed slightly, from approximately 1·8 Å in the native protein to approximately 2·2 Å in the denatured protein.

The small, calcium-binding protein, α-lactalbumin, is of particular interest for dynamics studies, since its structure, thermodynamic studies and function have been much discussed (McKenzie & White, 1991; Dobson, 1994; Kuwajima, 1996), and its denatured, molten globule and native states can be obtained with relative ease. Native α-lactalbumin has an α- and a β-domain with four disulphide bonds. The molten globule of α-lactalbumin is interesting because it is a prototype for studying partially folded intermediates. The protein can form a molten globule at low pH, in the absence of calcium ions at neutral pH, or even in absence of disulphide bonds (Griko & Remeta, 1999; Redfield *et al.* 1999). The structure of the α-lactalbumin molten globule and denatured states are highly heterogeneous. Denatured α-lactalbumin is easily obtained by dissolving the protein in 20 mM glycine (pH = 2) with or without 10 mM dithio-1,4-threitol (DTT), in 9 M urea solutions.

The internal dynamics of bovine α-lactalbumin (BLA) and its molten globules (MBLA) have also been examined using IQNS (Bu *et al.* 2000). The IQNS results showed lengthscale-dependent, picosecond-dynamics changes on lengthscales from 3·3 to 60 Å ($\Delta E \approx 70$ μeV; $0{\cdot}3\ \text{Å}^{-1} < Q < 1{\cdot}9\ \text{Å}^{-1}$). On shorter lengthscales, the non-exchangeable protons undergo jump motions over potential barriers, such as those involved in side-chain rotamer changes. The mean potential barrier to local jump motions is higher in BLA than in MBLA, as might be expected. On longer lengthscales, the protons undergo spatially restricted diffusive motions with the diffusive motions being more restricted in BLA than in MBLA. Both BLA and MBLA have similar mean square amplitudes of high-frequency motions comparable to the chemical bond vibrational motions. Bond vibrational motions thus do not change significantly upon folding. Interestingly, the quasielastic scattering intensities show pronounced maxima for both BLA and MBLA, suggesting that 'clusters' of atoms are moving collectively within the proteins on picosecond timescales. The correlation length, or 'the cluster size', of such atom clusters moving collectively is dramatically reduced in the molten globules with the correlation length being 6·9 Å in MBLA shorter than that of 18 Å in BLA. Similar collective motions may be important for the stability of the folded state, and may influence the protein folding pathways from the molten globules.

QENS experiments have been performed on the denatured bovine α-lactalbumin (DBLA) (Bu *et al.* 2001). The results showed that there are α-helical structures and tertiary-like side-chain interactions fluctuating on sub-nanosecond timescales under extremely denaturing conditions and even in the absence of disulphide bonds. Based on the lengthscale dependence of the decay rate of the measured correlation functions, the nanosecond dynamics of the native and the variously denatured proteins have three dynamic regimes. When $0{\cdot}05 < Q < 0{\cdot}5\ \text{Å}^{-1}$, the correlation time γ (see Section 4.1), shows a power law relationship, proportional to $Q^{(2{\cdot}42 \pm 0{\cdot}08)}$, which is analogous to the dynamic behaviour of a random coil. However, when $0{\cdot}5 < Q < 1{\cdot}0\ \text{Å}^{-1}$, the decay rate exhibits a γ proportional to $Q^{(1{\cdot}0 \pm 0{\cdot}2)}$ relationship. The effective

https://doi.org/10.1017/S0033583502003840 Published online by Cambridge University Press

diffusion constant of the protein decreases with increasing Q, a striking dynamic behaviour that is not found in any chain-like macromolecule. The authors suggested that the unusual dynamics are due to the presence of a strongly attractive force and collective conformational fluctuations in both the native and the denatured states of the protein. Above $Q > 1{\cdot}0$ Å^{-1} is a regime that displays the local dynamic behaviour of individual residues, γ proportional to $Q^{(1{\cdot}8 \pm 0{\cdot}3)}$. The picosecond timescale dynamics shows that the potential barrier to side-chain proton jump motion is reduced in the molten globule and in the denatured proteins when compared to that of the native protein. These results support the view that concurrent formation of secondary and tertiary structure clusters are established in the early stages of protein folding.

10. Acknowledgements

Moeava Tehei is supported by a doctorate grant from the Région Rhône-Alpes, France.

11. References

Adams, M. W. W. & Kelly, R. M. (1995). Enzymes from microorganisms in extreme environments. *Chem. Engng News* **18**, 32–42.

Andreani, C., Filabozzi, A., Menzinger, F., Desideri, A., Deriu, A. & Di Cola, D. (1995). Dynamics of hydrogen atoms in superoxide dismutase by quasielastic neutron scattering. *Biophys. J.* **68**, 2519–2523.

Angell, C. A. (1995). Formation of glasses from liquids and biopolymers. *Science* **267**, 1924–1935.

Arnold, F. H., Wintrode, P. L., Miyazaki, K. & Gershenson, A. (2001). How enzymes adapt: lessons from directed evolution. *Trends biochem. Sci.* **26**, 100–106.

Bée, M. (1988). *Quasielastic Neutron Scattering*. Bristol and Philadelphia: Adam Hilger.

Bellissent-Funel, M. C., Zanotti, J. M. & Chen, S. H. (1996). Slow dynamics of water molecules on the surface of a globular protein. *Faraday Discuss.* **103**, 281–294.

Bicout, D. J. & Zaccai, G. (2001). Protein flexibility from the dynamical transition: a force constant analysis. *Biophys. J.* **80**, 1115–1123.

Bizzarri, A. R., Paciaroni, A., Arcangeli, C. & Cannistraro, S. (2001). Low-frequency vibrational modes in proteins: a neutron scattering investigation. *Eur. Biophys. J.* **30**, 443–449.

Blatt, J. M. & Weisskopf, V. F. (1952). *Theoretical Nuclear Physics*, pp. 65–71. New York, London, Sydney: John Wiley & Sons.

Bon, C., Dianoux, A. J., Ferrand, M. & Lehmann, M. S. (2002). A model for water motion in crystals of lysozyme based on an incoherent quasi-elastic neutron scattering study. *Biophys. J.* **83**, 1578–1588.

Bon, C., Lehmann, M. S. & Wilkinson, C. (1999). Quasi-Laue neutron-diffraction study of the water arrangement in crystals of triclinic hen egg-white lysozyme. *Acta Crystallogr.* (*D*) **55**, 978–987.

Bonneté, F., Madern, D. & Zaccai, G. (1994). Stability against denaturation mechanisms in halophilic malate dehydrogenase 'adapt' to solvent conditions. *J. molec. Biol.* **244**, 436–447.

Bu, Z., Cook, J. & Callaway, J. E. (2001). Dynamic regimes and correlated structural dynamics in native and denatured α-lactalbumin. *J. molec. Biol.* **312**, 865–873.

Bu, Z., Neumann, D. A., Lee, S.-H., Brown, C. M., Engelman, D. M. & Han, C. C. (2000). A view of dynamics changes in the molten globule-native folding step by quasielastic neutron scattering. *J. molec. Biol.* **301**, 525–536.

Burton, R. E., Myers, J. K. & Oas, T. G. (1998). Protein folding dynamics: quantitative comparison between theory and experiment. *Biochemistry* **37**, 5337–5343.

Chan, H. S. & Dill, K. A. (1998). Protein folding in the landscape perspective: chevron plots and non-Arrhenius kinetics. *Proteins: Struct., Funct. Genet.* **30**, 2–33.

Conway, B. E. (1981). In *Studies in Physical and Theoretical Chemistry*, vol. 12. Amsterdam: Elsevier Science.

Cordone, L., Ferrand, M., Vitrano, E. & Zaccai, G. (1999). Harmonic behavior of trehalose-coated carbonmonoxy-myoglobin at high temperature. *Biophys. J.* **76**, 1043–1047.

Cordone, L., Galadja, P., Vitrano, E., Gassmann, A., Ostermann, A. & Parak, F. (1998). A reduction of protein specific motions in Co-ligated myoglobin embedded in a trehalose glass. *Eur. Biophys. J.* **27**, 173–176.

Daniel, R. M., Finney, J. L., Réat, V., Dunn, R., Ferrand, M., Smith, J. C., Dunn, R. V. & Finney, J. (1999). Enzyme dynamics and activity: time-scale dependence of dynamical transitions in glutamate dehydrogenase solution. *Biophys. J.* **77**, 2184–2190.

Debenedetti, P. G. & Stillinger, F. H. (2001). Supercooled liquids and the glass transition. *Nature* **410**, 259–267.

Dellerue, S., Petrescu, A. J., Smith, J. C. & Bellissent-Funel, M. C. (2001). Radially softening diffusive motions in a globular protein. *Biophys. J.* **81**, 1666–1676.

https://doi.org/10.1017/S0033583502003840 Published online by Cambridge University Press

Diehl, M., Doster, W., Petry, W. & Schober, H. (1997). Water-coupled low-frequency modes of myoglobin and lysozyme observed by inelastic neutron scattering. *Biophys. J.* **73**, 2726–2732.

Dobson, C. M. (1994). Protein folding. Solid evidence for molten globules. *Curr. Sci.* **4**, 636–640.

Doig, A. J. & Sternberg, M. J. (1995). Side-chain conformational entropy in protein folding. *Protein Sci.* **4**, 2247–2251.

Doster, W., Cusack, S. & Petry, W. (1989). Dynamical transition of myoglobin revealed by inelastic neutron scattering. *Nature* **337**, 754–756.

Doster, W., Cusack, S. & Petry, W. (1990). Dynamic instability of liquidlike motions in a globular protein observed by inelastic neutron scattering. *Phys. Rev. Lett.* **65**, 1080–1083.

Fermi, E. (1936). Sul moto dei neutroni nelle sostanze idrogenate. *La Ricerca Scientifica* **7**, 13–52.

Ferrand, M., Dianoux, A. J., Petry, W. & Zaccai, G. (1993a). Thermal motions and function of bacteriorhodopsin in purple membranes: effects of temperature and hydration studied by neutron scattering. *Proc. natn. Acad. Sci. USA* **90**, 9668–9672.

Ferrand, M., Petry, W., Dianoux, A. J. & Zaccai, G. (1993b). Dynamical transition of bacteriorhodopsin in purple membranes revealed by neutron scattering: a relation between structure, dynamics and function. *Physica A* **201**, 524–529.

Fisher, M. & Devlin, J. P. (1995). Defect activity in amorphous ice from isotopic exchange data: insight into the glass transition. *J. phys. Chem.* **99**, 11584–11590.

Fitter, J. (1999). The temperature dependence of internal molecular motions in hydrated and dry alpha-amylase: the role of hydration water in the dynamical transition of proteins. *Biophys. J.* **76**, 1034–1042.

Fitter, J., Ernst, O. P., Hauss, T., Lechner, R. E., Hofmann, K. P. & Dencher, N. A. (1998a). Molecular motions and hydration of purple membranes and disk membranes studied by neutron scattering. *Eur. Biophys. J.* **27**, 638–645.

Fitter, J. & Heberle, J. (2000). Structural equilibrium fluctuations in mesophilic and thermophilic alpha-amylase. *Biophys. J.* **79**, 1629–1636.

Fitter, J., Hermann, R., Dencher, N. A., Blume, A. & Hauss, T. (2001). Activity and stability of a thermostable alpha-amylase compared to its mesophilic homologue: mechanisms of thermal adaptation. *Biochemistry* **40**, 10723–10731.

Fitter, J., Lechner, R. E., Büldt, G. & Dencher, N. A. (1996a). Internal molecular motions of bacteriorhodopsin: hydration-induced flexibility studied by quasielastic incoherent neutron scattering using oriented purple membranes. *Proc. natn. Acad. Sci. USA* **93**, 7600–7605.

Fitter, J., Lechner, R. E. & Dencher, N. A. (1996b). Influence of lipids on the dynamical behaviour of bacteriorhodopsin in the purple membrane. In *Biological Macromolecular Dynamics* (eds. S. Cusack, H. Büttner, M. Ferrand, P. Langan & P. Timmins), pp. 123–127. Grenoble: Adenine Press.

Fitter, J., Lechner, R. E. & Dencher, N. A. (1996c). Temperature dependence of molecular motions in the membrane protein bacteriorhodopsin from QINS. *Physica* (*B*) **226**, 61–65.

Fitter, J., Lechner, R. E. & Dencher, N. A. (1997). Picosecond molecular motions in bacteriorhodopsin from neutron scattering. *Biophys. J.* **73**, 2126–2137.

Fitter, J., Verclas, S. A., Lechner, R. E., Bueldt, G., Ernst, O. P., Hofmann, K. P. & Dencher, N. A. (1999). Bacteriorhodopsin and rhodopsin studied by incoherent neutron scattering: dynamical properties of ground states and light activated intermediates. *Physica* (*B*) **266**, 35–40.

Fitter, J., Verclas, S. A., Lechner, R. E., Seelert, H. & Dencher, N. A. (1998b). Function and picosecond dynamics of bacteriorhodopsin in purple membrane at different lipidation and hydration. *FEBS Lett.* **433**, 321–325.

Frick, B. & Farago, B. (2002). Neutron spectroscopy by time-of-flight, backscattering and spin-echo techniques. In *Scattering: Scattering and Inverse Scattering in Pure and Applied Science* (eds. R. Pike & P. Sabatier), pp. 1209–1241. San Diego, San Francisco, New York, Boston, London, Sydney, Tokyo: Academic Press.

Gliss, C., Randel, O., Casalta, H., Sackmann, E., Zorn, R. & Bayerl, T. (1999). Anisotropic motion of cholesterol in oriented DPPC bilayers studied by quasielastic neutron scattering: The liquid-oriented phase. *Biophys. J.* **77**, 331–340.

Götze, W. & Sjögren, L. (1992). Relaxation processes in supercooled liquids. *Rep. Prog. Phys.* **55**, 241–376.

Griko, Y. V. & Remeta, D. P. (1999). Energetics of solvent and ligand-induced conformational changes in alpha-lactalbumin. *Protein Sci.* **8**, 554–561.

Guinier, A. & Fournet, G. (1955). *Small Angle Scattering of X-rays*. New York: John Wiley.

Iben, I. E., Braunstein, D., Doster, W., Frauenfelder, H., Hong, M. K., Johnson, J. B., Luck, S., Ormos, P., Schulte, A., Steinbach, P. J., Xie, A. H. & Young, R. D. (1989). Glassy behavior of a protein. *Phys. Rev. Lett.* **62**, 1916–1919.

Jaenicke, R. (2000). Do ultrastable proteins from hyperthermophiles have high or low conformational rigidity? *Proc. natn. Acad. Sci. USA* **97**, 2962–2964.

Johari, G. P., Hallbrucker, A. & Mayer, E. (1987). The glass–liquid transition of hyperquenched water. *Nature* **330**, 552–553.

Kanno, H., Speedy, R. J. & Angell, C. A. (1975). Supercooling of water to −92 °C under pressure. *Science* **189**, 880–881.

https://doi.org/10.1017/S0033583502003840 Published online by Cambridge University Press

Karplus, M. & Weaver, D. L. (1994). Protein folding dynamics: the diffusion–collision model and experimental data. *Protein Sci.* **3**, 650–668.

Klefhaber, T., Labhardt, A. M. & Baldwin, R. L. (1995). Direct NMR evidence for an intermediate preceding the rate-limiting step in the unfolding of ribonuclease A. *Nature* **375**, 513–515.

Kneller, G. R. & Smith, J. C. (1994). Liquid-like side-chain dynamics in myoglobin. *J. molec. Biol.* **242**, 181–185.

König, S., Bayerl, T. M., Coddens, G., Richter, D. & Sackmann, E. (1995). Hydration dependence of chain dynamics and local diffusion in L-α-dipalmitoylphosphatidylcholine multilayers studied by incoherent quasi-elastic neutron scattering. *Biophys. J.* **68**, 1871–1880.

König, S., Pfeiffer, W., Bayerl, T. M., Richter, D. & Sackmann, E. (1992). Molecular dynamics of lipid bilayers studied by incoherent quasi-elastic neutron scattering. *Journal de Physique II* **2**, 1589–1615.

Kuntz, Jr., I. D. & Kauzmann, W. (1974). Hydration of proteins and polypeptides. *Adv. Protein Chem.* **28**, 239–345.

Kuwajima, K. (1996). The molten globule state of alpha-lactalbumin. *FASEB J.* **10**, 102–109.

Lechner, R. E., Dencher, N. A., Fitter, J. & Büldt, G. (1992). Proton dynamics in a 2D-'Single Crystal' of bacteriorhodopsin. *Physica Scripta* **T45**, 236–241.

Lechner, R. E., Fitter, J., Dencher, N. A. & Hauss, T. (1998). Dehydration of biological membranes by cooling: an investigation on the purple membrane. *J. molec. Biol.* **277**, 593–603.

Lehnert, U., Réat, V., Weik, M., Zaccai, G. & Pfister, C. (1998). Thermal motions in bacteriorhodopsin at different hydration levels studied by neutron scattering: correlation with kinetics and light-induced conformational changes. *Biophys. J.* **75**, 1945–1952.

Levine, Y. K., Bailey, A. I. & Wilkins, M. H. (1968). Multilayers of phospholipid bimolecular leaflets. *Nature* **220**, 577–578.

Madigan, M. T. & Marrs, B. L. (1997). Extremophiles. *Scient. Am.* **276**, 82–87.

Mayo, K. H., Parak, F. & Mössbauer, R. L. (1981). Observations of elastic and quasi-elastic nuclear gamma resonance absorption in hemoglobin crystals. *Phys. Lett.* **82A**, 468–470.

Melchers, B., Knapp, E. W., Parak, F., Cordone, L., Cupane, A. & Leone, M. (1996). Structural fluctuations of myoglobin from normal-modes, Mössbauer, Raman and absorption spectroscopy. *Biophys. J.* **70**, 2092–2099.

Mevarech, M. & Neumann, E. (1977). Malate dehydrogenase isolated from extremly halophilic bacteria of the Dead Sea. 2. Effect of salt on catalytic activity and structure. *Biochemistry* **16**, 3786–3792.

McKenzie, H. A. & White, Jr., F. H. (1991). Lysozyme and alpha-lactalbumin: structure, function and interrelationships. *Adv. Protein Chem.* **41**, 173–315.

McMillan, J. A. & Los, S. C. (1965). Vitreous ice: irreversible transformations during warm-up. *Nature* **206**, 806–807.

Middendorf, H. D., Hayward, R. L., Parker, S. F., Bradshaw, J. & Miller, A. (1995). Vibrational neutron spectroscopy of collagen and model polypeptides. *Biophys. J.* **69**, 660–673.

Mishima, A. & Stanley, H. E. (1998). The relationship between liquid, supercooled and glassy water. *Nature* **396**, 329–335.

Nemethy, G. & Scheraga, H. A. (1964). Structure of water and hydrophobic bonding in proteins. IV. The thermodynamic properties of lipid deuterium oxide. *J. chem. Phys.* **41**, 680–689.

Orecchini, A., Paciaroni, A., Bizzarri, A. R. & Cannistraro, S. (2001). Low-frequency vibrational anomalies in β-lactoglobulin: contribution of different hydrogen classes revealed by inelastic neutron scattering. *J. phys. Chem.* (*B*) **105**, 12150–12156.

Oren, A. (1986). Intracellular salt concentrations of the anaerobic halophilic eubacteria *Haloanaerobium praevalens* and *Halobacteroides halobius*. *Can. J. Microbiol.* **32**, 4–9.

Paciaroni, A., Stroppolo, M. E., Arcangeli, C., Bizzarri, A. R., Desideri, A. & Cannistraro, S. (1999). Incoherent neutron scattering of copper azurin: a comparison with molecular dynamics simulation results. *Eur. Biophys. J.* **28**, 447–456.

Parak, F. (In Press). *Rep. Prog. Phys.*

Parak, F., Knapp, E. W. & Kucheida, D. (1982). Protein dynamics: Mössbauer spectroscopy on deoxymyoglobin crystals. *J. molec. Biol.* **161**, 177–194.

Pérez, J., Zanotti, J. M. & Durand, D. (1999). Evolution of the internal dynamics of two globular proteins from dry powder to solution. *Biophys. J.* **77**, 454–469.

Ptitsyn, O. B. (1995). Molten globule and protein folding. *Adv. Protein Chem.* **47**, 83–229.

Portman, J. J., Takada, S. & Wolynes, P. G. (2001). Microscopic theory of protein folding rates. II. Local reaction coordinates and chain dynamics. *J. chem. Phys.* **114**, 5082–5096.

Réat, V., Dunn, R., Ferrand, M., Finney, J. L., Daniel, R. M. & Smith, J. C. (2000). Solvent dependence of dynamic transitions in protein solutions. *Proc. natn. Acad. Sci. USA* **97**, 9961–9966.

Réat, V., Patzelt, H., Pfister, C., Ferrand, M., Oesterhelt, D. & Zaccai, G. (1998). Dynamics of different functional parts of bacteriorhodopsin: H–^{2}H labelling and neutron scattering. *Proc. natn. Acad. Sci. USA* **95**, 4970–4975.

Réat, V., Zaccai, G., Ferrand, M. & Pfister, C. (1997). Functional dynamics in purple membrane. In *Biological Macromolecular Dynamics* (eds. S. Cusack, H. Büttner, M. Ferrand, P. Langan & P. Timmins), pp. 117–122. Schenectady, NY, USA: Adenine Press.

https://doi.org/10.1017/S0033583502003840 Published online by Cambridge University Press

Receveur, V., Calmettes, P., Smith, J. C., Desmadril, M., Coddens, G. & Durand, D. (1997). Picosecond dynamical changes on denaturation of yeast phosphoglycerate kinase revealed by quasielastic neutron scattering. *Proteins: Struct., Funct. Genet.* **28**, 380–387.

Redfield, C., Schulman, B. A., Mihollen, M. A., Kim, P. S. & Dobson, C. M. (1999). Alpha-lactalbumin forms a compact molten globule in the absence of disulfide bonds. *Nature struct. Biol.* **6**, 948–952.

Rupley, J. A. & Careri, G. (1991). Protein hydration and function. *Adv. Protein Chem.* **41**, 37–172.

Rupley, J. A., Gratten, E. & Careri, G. (1983). Water and globular proteins. *Trends biochem. Sci.* **8**, 18–22.

Scherbakova, I. V., Zgurskaya, E. I., Fan, L. X., Serdyuk, I. N. & Zaccai, G. (1997). Metabolic regulation of selective deuterium incorporation into RNA and protein components of the ribosome. In *Biological Macromolecular Dynamics* (eds. S. Cusack, H. Büttner, M. Ferrand, P. Langan & P. Timmins), pp. 165–169. New York: Adenine Press.

Sears, V. F. (1986). Electromagnetic neutron-atom interactions. *Phys. Rep.* **5**, 281–317.

Settles, M. & Doster, W. (1996). Anomalous diffusion of adsorbed water: a neutron scattering study of hydrated myoglobin. *Faraday Discuss.* **103**, 269–279.

Smith, J. C. (1991). Protein dynamics: comparison of simulations with inelastic neutron scattering experiments. *Q. Rev. Biophys.* **24**, 227–291.

Smith, R. S. & Kay, B. D. (1999). The existence of supercooled liquid water at 150 K. *Nature* **398**, 788–791.

Tarek, M. & Tobias, D. J. (2000). The dynamics of protein hydration water: a quantitative comparison of molecular dynamics simulations and neutron-scattering experiments. *Biophys. J.* **79**, 3244–3257.

Tehei, M., Madern, D., Pfister, C. & Zaccai, G. (2001). Fast dynamics of halophilic malate dehydrogenase and bovine serum albumin measured by neutron scattering under various solvent conditions influencing protein stability. *Proc. natn. Acad. Sci. USA* **98**, 14356–14361.

Tsai, A. M., Neumann, D. A. & Bell, L. N. (2000). Molecular dynamics of solid-state lysozyme as affected by glycerol and water: a neutron scattering study. *Biophys. J.* **79**, 2728–2732.

Tsai, A. M., Udovic, T. J. & Neumann, D. A. (2001). The inverse relationship between protein dynamics and thermal stability. *Biophys. J.* **81**, 2339–2343.

Volino, F. & Dianoux, A. J. (1980). Neutron incoherent scattering law for diffusion in a potential of spherical symmetry: general formalism and application to diffusion inside a sphere. *Molec. Phys.* **41**, 271–279.

Weik, M., Patzelt, H., Zaccai, G. & Oesterhelt, D. (1998). Localization of glycolipids in membranes by in-vivo labelling and neutron diffraction. *Molec. Cell* **1**, 411–419.

Wright, P. E. & Dyson, H. J. (1999). Intrinsically unstructured proteins: r-assessing the protein structure–function paradigm. *J. molec. Biol.* **293**, 321–331.

Yang, P. H. & Rupley, J. A. (1979). Protein–water interactions. Heat capacity of the lysozyme–water system. *Biochemistry* **18**, 2654–2661.

Yellow Book ILL: http://www.ill.fr/pages/science/IGroups/yb.pdf

Zaccai, G. (1987). Structure and hydration of purple membranes in different conditions. *J. molec. Biol.* **194** (3), 569–572.

Zaccai, G. (2000a). How soft is a protein? A protein force constant measured by neutron scattering. *Science* **288**, 1604–1607.

Zaccai, G. (2000b). Moist and soft, dry and stiff: a review of neutron experiments on hydration-dynamics-activity relations in the purple membrane of *Halobacterium salinarum*. *Biophys. Chem.* **86**, 249–257.

Zaccai, G., Tehei, M., Scherbakova, I., Serdyuk, I., Gerez, C. & Pfister, C. (2000). Incoherent elastic neutron scattering as a function of temperature: a fast way to characterise in-situ biological dynamics in complex solutions. *Journal de Physique IV* **10**, Pr7-283–287.

Zanotti, J. M., Bellissent-Funel, M. C. & Parello, J. (1999). Hydration-coupled dynamics in proteins studied by neutron scattering and NMR: the case of the typical EF-hand calcium-binding parvalbumin. *Biophys. J.* **76**, 2390–2411.

https://doi.org/10.1017/S0033583502003840 Published online by Cambridge University Press